Adsorption Behavior of Acidic and Basic Proteins onto Citrate-Coated Au Surfaces Correlated to Their Native Fold, Stability, and pI

ARTICLE *in* THE JOURNAL OF PHYSICAL CHEMISTRY B · DECEMBER 2007

Impact Factor: 3.3 · DOI: 10.1021/jp074839d · Source: PubMed

Adsorption Behavior of Acidic and Basic Proteins onto Citrate-Coated Au Surfaces Correlated to Their Native Fold, Stability, and pI

Wilhelm R. Glomm,*,† Øyvind Halskau, Jr.,‡ Ann-Mari D. Hanneseth,† and Sondre Volden†

Ugelstad Laboratory, Department of Chemical Engineering, Norwegian University of Science and Technology (NTNU), N-7491 Trondheim, Norway and Department of Biochemistry and Molecular Biology, University of Bergen, Jonas Lies vei 91, N-5009 Bergen, Norway

Received: June 21, 2007; In Final Form: September 21, 2007

The adsorption of eight different proteins (α-lactalbumin (types I and III), bovine serum albumin, hemoglobin, myoglobin, cytochrome *c*, α-casein, and lysozyme) onto a model anionic surface was performed at equivalent bulk (solvent, ionic strength, pH) and surface conditions. Adsorption was monitored on a quartz crystal microbalance with dissipation monitoring (QCM-D) with citrate-coated gold surfaces as adsorbents and has been correlated to native fold stability determined from near- and far-UV circular dichroism (CD) measurements. The proteins studied here were chosen based on their pI and documented knowledge about their structural stability and flexibility. Protein adsorption was found to be independent of global protein charge. Rather, binding occurs through oppositely charged patches on protein and surface. Moreover, data indicate that there is a correlation between secondary and tertiary structure stability and the adsorption characteristics at interfaces. Also, protein surface coverage, layer thickness, and flexibility can be tuned as a function of deposition method. This is discussed in terms of adsorption/spreading kinetics and intermolecular (protein−surface and protein−protein) interactions. Adsorption to surfaces can induce formation of supramolecular structures such as micelles (in the case of α-Cas) and multilayers (as for Hb). In the case of α-casein, this phenomenon depends on the deposition method and protein concentration. When ranking the surface coverage for proteins added in excess, the order is Lyz < Cyt *c* < Mb < BSA < α-La I < α-Cas < α-La III < Hb, which can be correlated to the proteins ability to form supramolecular structures (α-Cas, Hb), overall conformational flexibilities, and ability to form stable intermediates.

Introduction

Protein adsorption is a complex process involving van der Waals, hydrophobic, and electrostatic interactions, hydrogen bonding, and rearrangement in the protein structure (for a review, see, e.g., Norde[1]). Protein adsorption characteristics can be controlled by altering substrate surface parameters such as chemistry, size, and curvature.[2,3] However, the extent to which these factors contribute to the control of conformation and thus to the activity of surface-confined proteins is not yet fully understood. In order to gain further insight into the complex behavior of protein adsorption from body fluids, simple single-protein model systems are necessary. Recently, Brewer et al. reported the adsorption of bovine serum albumin (BSA) onto bare and citrate-coated Au surfaces and citrate-stabilized Au nanoparticles using QCM-D and ζ-potential vs pH measurements.[4] Here, the surface coverage Γ of BSA on bare (hydrophobic) Au surfaces was found to be about twice the surface coverage of BSA on a citrate-coated Au surface, indicating that on bare Au BSA binds by a denaturation process through which hydrophobic groups within the protein are exposed to the surface.

The details of the driving forces behind protein−surface interactions and the relationship between protein conformation, dynamics, and electrostatic and hydrophobic properties in its native (bulk solution) and adsorbed states require further clarification. Some proteins, for example cytochrome *c*,[5] plastocyanine[6] and α-lactalbumin,[7] display an affinity for lipid membranes which in some cases and under some conditions can be classified as reversible.[8] Such reversible behavior may have a bearing on the more general adsorption to a wide range of metal or polymer surfaces. Soluble, globular proteins consist of a hydrophobic core and a charged surface that may interact favorably with the solvent. Detailed structural characterization of proteins adsorbed on surfaces is not a trivial matter. However, it is generally believed that the protein will interact efficiently with a surface if it can rearrange its conformation to optimize favorable interactions between itself and the surface and the surface−solvent interface.[9] Many reports indicate that proteins form so-called molten globule (MG) conformations at the interface,[10,11] an intermediately folded protein state that is usually defined as having solvent-exposed hydrophobic patches and a native-like secondary structure and lacking fixed tertiary structure.[12] Thus, proteins that are able to form the flexible molten globule state are predicted to bind efficiently to surfaces.

Adsorption of proteins on solid surfaces is of relevance to a wide audience due to its many possible impacts on systems such as medical implants, biochips and biosensors, drug delivery, and food and biochemical processing (see, e.g., Kasemo[13] or Malmsten[14] for a review). Nevertheless, different properties of the adsorbed proteins are required for each application. Specific arrangement and conformation of adsorbed proteins on biochips are, for example, essential in order to ensure good biofunction-

* To whom correspondence should be addressed. Fax: +47 73 59 40 80. E-mail: glomm@nt.ntnu.no.
† Norwegian University of Science and Technology.
‡ University of Bergen.

10.1021/jp074839d CCC: $37.00
Published on Web 12/06/2007

ality of the sensor surface and, subsequently, the best precision of analytical results. Different implants will also require different adhesion qualities of adsorbed proteins. For catheters and contact lenses poor protein adhesion is demanded, whereas for bone implants, strong adhesion is necessary in order to build a compact bone−implant interface. For targeted drug delivery applications, the protein can act both as a stabilizing agent and as a scaffold for active species such as cell-targeting peptides.[15,16]

Immobilization of proteins such as antibodies or enzymes, with simultaneous conservation of their activities, may give rise to the development of new functional surfaces suitable for use in many fields including biosensors and development of catalytic and biocompatible devices. The latter is typically denoted as any material which is nontoxic, chemically and physically stable, and nonimmunogenic.[17] Biocompatibility is closely related to cell behavior on contact with implant surfaces and is decided by two factors: the response of the host to the implant and the response of the implant in the host.[2,13] It is generally believed that when a surface is exposed to a biofluid — consisting primarily of proteins and water — the solid−liquid interface dictates the subsequent system (e.g., organism) response to the surface. Consequently, much research has been devoted to methods that modify the surfaces of existing biomaterials in order to achieve more desirable biological integration. Understanding and eventually controlling protein adsorption characteristics is therefore essential in order to develop new generations of materials with improved biocompatibility and functionality.

Materials and Methods

Materials. *Holo* bovine α-lactalbumin (type 1, calcium-saturated, α-La I), *apo* bovine α-lactalbumin (type 3, calcium depleted, α-La III), chicken egg white lysozyme, bovine α-casein, bovine heart cytochrome *c*, horse heart myoglobin, rabbit hemoglobin, bovine serum albumin, and trisodium citrate (hereafter referred to as citrate) were all obtained from Sigma-Aldrich. All chemicals were used without further purification.

QCM-D Measurements. The Au-coated QCM crystals were AT-cut quartz crystals (KSV Instruments Ltd.) with a fundamental frequency (f_0) of 5 MHz and an active sensor area of 20 mm^2. The gold crystals were cleaned in a Piranha solution consisting of H_2SO_4 (98%) and H_2O_2 (30%) in a 3:1 ratio for approximately 30 min followed by rinsing with Milli-Q water and drying under a stream of N_2 gas. All crystals were used immediately after preparation.

Mass adsorption data were acquired at 20, 25, 37, and 50 °C on a QCM-Z500 supplied by KSV Instruments Ltd., which monitors the frequency changes of a piezoelectric crystal as a function of time when exposed to an adsorbing species. For more information about the QCM and QCM-D techniques, see, e.g., the review by Marx[18] and references therein. The adsorbed mass (surface coverage) for each species was calculated using the Sauerbrey equation (eq 1) on data extracted from the third harmonic (unless otherwise noted) of the resonance

$$\Delta m = -\frac{C\Delta f}{n} \qquad \text{(eq 1)}$$

in which Δm is the change in mass, C is the sensitivity constant (17.8 ng cm^{-2} Hz^{-1}), Δf is the shift in frequency, and n is the number of the harmonic.[19] The surface coverage thus calculated is however to be considered as an approximation as there will be additional mass registered from water trapped within or associated with the adsorbed layer.[20−22] Moreover, rigidity and thickness of adsorbed layers can also be observed through this technique. This was done both by observing the dissipation changes ΔD and by directly fitting the data acquired from the QCM measurements in the software supplied by KSV. The dissipation factor D is defined by

$$D = \frac{E_{\text{diss}}}{2\pi E_{\text{stor}}} \qquad \text{(eq 2)}$$

where E_{diss} is the total dissipated energy during one oscillation cycle and E_{stor} is the total energy stored in the oscillation. With the QCM-Z500, the dissipation changes following adsorption, $\Delta D = D - D_0$, where D_0 is the dissipation factor of the precoated crystal immersed in the solvent and can be continuously measured during the adsorption process. Here, the precoating of the crystal (with citrate) consists of exposing the crystal to a 10 mM citrate solution and allowing it to equilibrate until no further frequency changes can be observed prior to introduction of the protein solutions.

In this study, frequency and dissipation responses were recorded at 5, 15, 25, 35, 45, and 55 MHz, corresponding to the fundamental frequency and the harmonics $n = 3$, 5, 7, 9, and 11. For clarity, only the normalized frequency shifts, $\Delta f_{\text{normalized}} = \Delta f_n/n$, and the dissipation shifts, ΔD, for the third harmonic (unless otherwise noted) are represented. Data at other harmonics are included for calculation of the effective layer thickness, which was directly calculated using the software supplied by KSV Instruments Ltd.

We used two experimental protocols, as previously described by Brewer[4] et al.: sequential deposition and direct deposition. Citrate is a common and convenient electrostatic stabilizing agent for gold nanoparticles as the particles are typically synthesized though a citric acid reduction reaction (the Turkevich method).[23−25] For gold nanoparticles, electrostatic stabilization arises from a mutual repulsion between neighboring colloids as a result of the negative surface charge imparted by the citrate layer. Under the experimental conditions used here the zeta potential of 10 nm citrate-coated Au nanoparticles is −45 mV.[4] Citrate has also been used as a dispersant for aqueous alumina suspensions.[26] For both experimental protocols, the crystal was precoated with citrate (10 mM in water, pH 8.55) prior to introducing the proteins. This was done by exposing the Au-coated crystal to a solution of citrate (10 mM in water, pH 8.55) and allowing it to equilibrate for approximately 30 min, after which the citrate concentration was kept constant. In the sequential deposition measurement, successive aliquots of protein were added sequentially to a single citrate-coated Au crystal, ranging from low to high concentration (∼1−50 μM in 10 mM citrate), and a citrate wash was performed after each measurement. We assumed the system to have reached equilibrium when the frequency change was smaller than 1 Hz per 5 min (baseline noise). All sequential depositions were carried out at 25 °C. In the direct deposition measurement, a protein solution (∼30 μM in 10 mM citrate) was deposited onto a freshly prepared citrate-coated gold slide for each measurement. Direct measurements were performed for all proteins at 25 and 37 °C. Other temperatures were also investigated for some of the proteins (Mb, Hb, and α-Cas) on the basis of the CD spectra (see Table 3).

For the sequential depositions, mass values acquired from the Sauerbrey equation were fitted using the Langmuir adsorption isotherm

$$\Gamma_{\text{adsorbate}} = \frac{\Gamma_{\max} K[S]_{\text{free}}}{1 + K[S]_{\text{free}}} \qquad \text{(eq 3)}$$

TABLE 1: Protein Adsorption Data Collected at 25 °C Using the Sequential Deposition Method[a]

protein	$-\Delta f_{max}$ (Hz)	proteins/cm^2 ($\times 10^{12}$)	ΔD ($\times 10^{-6}$)	$\lvert\Delta D/\Delta f_{max}\rvert$ ($\times 10^{-9}$ Hz^{-1})	thickness[b] (nm)	$\Gamma_{Langmuir}$[c] ($\times 10^{12}$)	K[c] (μM^{-1})
α-La I	14 ± 1	11 ± 1	0.15	9.6	2.9 RF	12.2 ± 0.4	0.4 ± 0.1
α-La III	10.6 ± 0.2	7.9 ± 0.2	0.54	46.0	1.5 RF	9.3 ± 0.3	0.32 ± 0.05
Lyz	5 ± 2	3 ± 1	0.80	132.6	1.2 VF	5.5 ± 0.3	0.4 ± 0.2
Cyt *c*	17.0 ± 0.5	13.8 ± 0.4	0.19	11.3	5.0 RF	18 ± 1	0.14 ± 0.04
BSA	20.7 ± 0.5	3.3 ± 0.1	1.33	62.5	3.3 RF	3.8 ± 0.1	0.27 ± 0.06
Mb	21.3 ± 0.6	13.1 ± 0.4	0.70	32.4	4.8 RF	17 ± 1	0.12 ± 0.04
Hb	220 ± 27	36 ± 4	40.15	156.5	72.4[d]	N/A	N/A
α-Cas	68 ± 3	22 ± 1	3.07	43.2	14.8 VF	22.9 ± 0.1	2.7 ± 0.4

[a] Listed values correspond to the maximum obtained surface coverage. The data points are averaged over the third, fifth, seventh, and ninth harmonics of the resonance frequency with the corresponding standard deviations. Frequency shifts have been normalized with respect to the harmonic at which they have been collected. [b] Determined using the accompanying software. RF and VF refer to rigid film and viscoelastic film, respectively, according to whether frequency changes overlap when normalized with respect to harmonic. [c] Calculated using eq 3 to yield proteins/cm^2 for the fit. [d] Found to be composed of one rigid layer (6.6 nm) for low concentrations and one viscoelastic layer (65.8 nm) at higher Hb concentrations.

TABLE 2: Protein Adsorption Data Collected Using the Direct Deposition Method[a]

protein	temperature (°C)	$-\Delta f_{max}$ (Hz)	proteins/cm^2 ($\times 10^{12}$)	ΔD ($\times 10^{-6}$)	$\lvert\Delta D/\Delta f_{max}\rvert$ ($\times 10^{-9}$ Hz^{-1})	thickness[b] (nm)
α-La I	25	15 ± 1	11.1 ± 0.5	1.02	66.7	2.4 RF
	37	15 ± 2	11 ± 1	5.82	391.7	3.1 RF
α-La III	25	20 ± 1	15.1 ± 0.7	2.19	103.4	2.9 RF
	37	14.5 ± 0.8	10.8 ± 0.6	−0.81	52.6	2.3 RF
Lyz	25	30.0 ± 0.4	22.1 ± 0.3	0.50	16.6	5.5 VF
	37	24.3 ± 0.8	18.0 ± 0.6	0.08	3.4	5.1 VF
Cyt *c*	25	24 ± 1	21 ± 1	0.68	26.6	3.8 RF
	37	28 ± 4	24 ± 4	−0.34	14.0	4.1 RF
BSA	25	31 ± 1	5.0 ± 0.2	1.22	38.8	5.8 RF
	37	25 ± 2	4.0 ± 0.3	1.37	50.1	4.2 RF
Mb	25	29.7 ± 0.8	18.2 ± 0.5	0.98	32.0	4.8 RF
	37	26 ± 1	16.0 ± 0.5	0.72	28.7	4.6 RF
	50	22 ± 5	14 ± 3	−0.01	0.5	4.2 RF
Hb	20	240 ± 58	40 ± 9	39.47	125.8	50.7 VF
	25[c]	534 ± 80	88 ± 15	137.68	257.8	172.6 VF
	37	383 ± 60	63 ± 10	92.3	199.2	112.6 VF
α-Cas	20	66 ± 2	21 ± 1	6.82	98.8	34.7 VF
	25	82 ± 6	26 ± 2	8.39	95.0	29.9 VF
	37	77 ± 4	24 ± 1	7.98	96.4	15.6 VF

[a] Listed values correspond to equilibrium coverage at protein bulk concentration of ~30 μM. Data is averaged over multiple experiments and harmonics. [b] Layer thickness determined using the accompanying software. RF and VF refer to rigid film and viscoelastic film, respectively, according to whether frequency changes overlap when normalized with respect to harmonic. [c] Result obtained after 20 h of equilibration.

and binding constants for the different proteins were calculated. In eq 3, $\Gamma_{adsorbate}$ denotes the surface coverage of the adsorbate (protein), Γ_{max} is the maximum surface coverage, and K is a binding constant equal to the ratio of adsorption and desorption rate constants ($K = k_a/k_d$).

Dynamic Interfacial Tension Measurements. In order to determine the critical micelle concentration (CMC) of α-casein in a 10 mM citrate buffer at 25 °C, we performed a series of interfacial tension measurements to determine the aggregation state of the protein (single molecules vs micelles) under the experimental conditions.

The drop tensiometer (CAM 200 KSV Instruments, Finland) was used to measure the interfacial tension of α-casein by analyzing the axial symmetric shape (Laplacian profile) of a water droplet in air. All measurements were performed at room temperature. A water droplet was created from a needle connected to a syringe (1 mL). Images were recorded continuously at a rate of 1 image per second for 30 min after creating the air−water interface. α-Casein was dissolved in citrate buffer (10 mM) to a concentration of 1×10^{-4} M and further diluted to solutions with concentrations ranging from 1×10^{-7} to 1×10^{-4} M.

Circular Dichroism Measurements. Circular dichroism (CD) measurements were performed with a Jasco J-810 spectropolarimeter equipped with a PTC-348WI Peltier element for temperature control. Far-UV CD measurements (yielding information about the secondary structure through differences in absorption of the left- and right-circularly polarized components of plane-polarized light absorbing at wavelengths corresponding to the peptide bond)[27] were performed using a quartz cell with a path length of 1 mm. Sample concentrations of 0.06 mg/mL (median protein concentration 8.8 μM) protein in 10 mM citrate, pH 8.55, were used. Protein thermal denaturation was monitored by following the changes in ellipticity at 222 nm with a scan rate of 2 °C/min in the 10−90 °C temperature range. Protein concentration was measured by UV absorption at 280 nm using the formula $A_{280} = C \cdot l \cdot E_{280}$, where A_{280} is the absorbance at 280 nm, C is the protein concentration in mol·L^{-1}, l is cuvette path length in cm, and E_{280} is the extinction coefficient in mol^{-1}·L·cm^{-1}. E_{280} was estimated for Mb, Hb, and α-Cas using the formula $E_{280} = \#W \cdot 5500 + \#Y \cdot 1490 + \#CC \cdot 125$, where *#W*, *#Y*, and *#CC* represent the number of tryptophans, tyrosine, and disulfide bridges in the protein, respectively.[28] Experimental values of E_{280} for α-La (I and III), Lyz, Cyt *c*, and BSA were taken from the literature.[28,29] Near-UV CD measurements (yielding information about the environment of the aromatic acid residues; for tightly folded proteins these environments are usually chiral and give rise to a difference in absorption of the left and right components of incident light)[27] were performed using quartz cells with path lengths of 5 mm. The sample concentration used was 1 mg/mL (median protein concentration 142 μM) in 10 mM citrate, pH = 8.55. For each protein, CD

TABLE 3: Transition Temperatures (°C) for α-Helix and Tertiary Structure Determined by Far- and Near-UV CD Spectroscopy[a]

	α-helix		tertiary structure		
protein	main transition	minor transitions	main transition	minor transitions	mean residual ellipticity at 222 nm and 25 °C, θ = deg·cm^2·dmol^{-1} × 10^{-3}
α-La I	45−55[c]		49		−5.6
α-La III	c		38		−8.5
Lyz	73	35	∼80[e]		−9.0
Cyt *c*	∼82		∼80[e]		−6.3
BSA	58	23, 37	64		−14.4
Mb	81	21, 34	f		−3.0
Hb	58−60[b]		∼55[d]		−15.0
α-Cas	c		f		−6.9

[a] Major transitions are reported as the maxima of the first derivative of temperature scan CD data at a wavelength of 222 nm. Minor transitions are first-derivative local maxima with function values lower than the main transition. Mean residual ellipticity at 222 nm and 25 °C is given in the rightmost column. [b] Broad and unresolved peak. [c] The first derivative of the protein temperature scan curve did not yield clear peaks. [d] There is a minimum in ellipticity around 35 °C. The temperature−ellipticity dependence is very weak with a general loss of ellipticity as the temperature increases. [e] First-derivative peak had not reached the maximum when the signal became random scatter, probably due to onset of heat-induced precipitation. [f] No discernible CD signals were found in the 260−290 nm range for this protein.

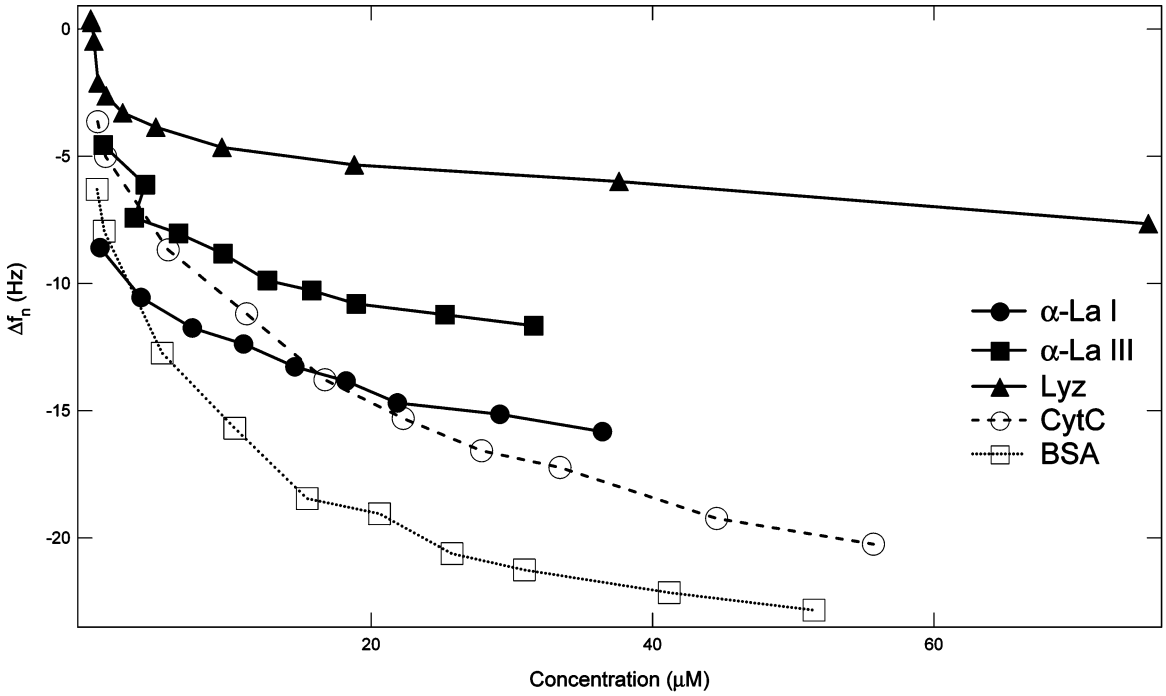

Figure 1. Normalized averaged frequency shifts (acquired at the third, fifth, seventh, and ninth harmonics of the fundamental) as a function of concentration during sequential adsorption of α-La I, α-La III, Lyz, Cyt *c*, and BSA at 25 °C.

spectra in the 260−290 nm range were acquired, and a wavelength was chosen corresponding to the maximum signal in this range. A temperature scan was subsequently performed on the protein at this wavelength. Temperature scans were performed at 10−90 °C using a scan rate of 2 °C/min. α-Cas and Mb did not have discernible optical rotation in this region, and near-UV temperature scans were not performed for these proteins. No calculation of mean residual ellipticity was performed for near-UV data as it is difficult to link CD signals in this range to individual residues. Data analysis: Appropriate blanks were subtracted, and data was analyzed in Sigmaplot. First derivatives of the temperature−signal function were calculated as $\Delta s/\Delta T = (s_2 - s_1)/(T_2 - T_1)$, where s is the dichroism signal and T is the temperature. Subscripts 1 and 2 refer to measurement points at temperatures T and $T + 10$ °C, respectively. The resulting derivative was plotted against $(T_1 + T_2)/2$. Negative exponential smoothing using a sampling range of 0.1 and polynomial degree of 1 was applied to temperature scan data points and to first-derivative plots for clarity when reading plot values presented in Table 3.

Results

Sequential Deposition of Proteins. Averaged normalized frequency shifts (of the third, fifth, seventh, and ninth harmonics of the fundamental frequency) as a function of protein bulk concentrations are shown in Figures 1 and 2. With the exception of Hb, all proteins studied here only displayed a single saturation plateau, indicating that the adsorption did not proceed beyond monolayer coverage (see, e.g., Malmsten,[14] Chapters 1 and 4). If the initial adsorbed layer can act as a substrate for further (for example, physical) adsorption, then instead of the isotherm leveling off to some saturated value (i.e., "monolayer") it would be expected to rise indefinitely. Subsequent rinsing with buffer (10 mM citrate) and H_2O did not induce significant frequency or dissipation changes, which is consistent with irreversible adsorption. Collected and calculated protein adsorption data using the sequential deposition method at 25 °C are listed in Table 1. Listing the normalized frequency shifts at maximum surface coverage (Δf_{max}) in increasing order, the proteins can be ranked as Lyz (∼5 Hz) < α-La III < α-La I < Cyt *c* <

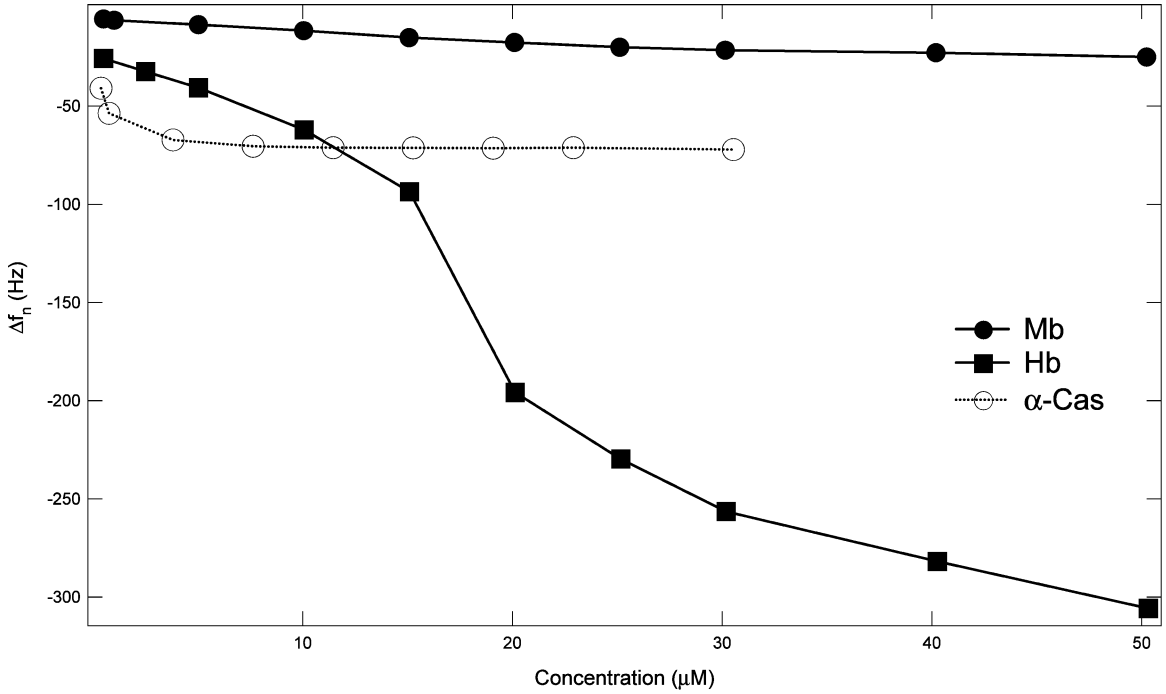

Figure 2. Normalized averaged frequency shifts (acquired at the third, fifth, seventh, and ninth harmonics of the fundamental) as a function of concentration during sequential adsorption of Mb, Hb, and α-Cas at 25 °C.

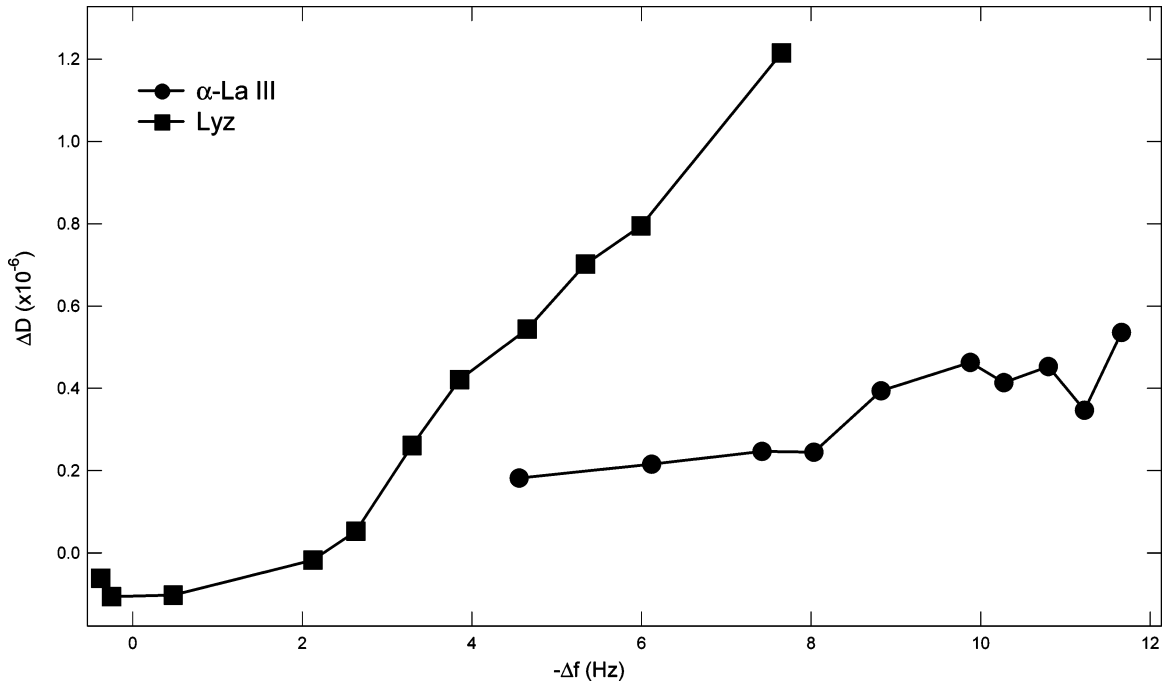

Figure 3. *D*−*f* plots for the sequential adsorption of α-La III and Lyz at 25 °C.

BSA ≤ Mb < α-Cas < Hb (∼220 Hz). The adsorption data were fit to the Langmuir model (eq 3) with resulting Γ_{max} and *K* values listed in Table 1. The calculated Γ_{max} values (from the Langmuir model) correspond well to the experimentally determined maximum surface coverage (from the maximum frequency shifts) for the proteins studied here (Hb excluded). From the calculated *K* values, the surface affinities of the proteins in 10 mM citrate (pH = 8.55) at 25 °C can be listed as (in increasing order) Mb < Cyt *c* < BSA < α-La III < α-La I ≅ Lyz ≪ α-Cas.

In order to get a measure of the relative flexibilities of the adsorbed layers for the different proteins at maximum surface coverage, the ratio between normalized frequency and dissipation shifts, $|\Delta D/\Delta f_{max}|$ (the induced energy loss per coupled unit mass), was assessed (Table 1). Here, the flexibility of the adlayer is proportional to the $|\Delta D/\Delta f_{max}|$ ratio[17,30] with α-La I forming the most rigid layer and Hb forming the most flexible. To relate the observed changes in Δ*D* to changes in Δ*f* as they occurred throughout the experiment, we show representative Δ*D* vs Δ*f* plots (hereafter referred to as *D*−*f* plots) for α-La III, Lyz, Hb, and α-Cas in Figures 3−5. For the sequential deposition method, plotting Δ*D* vs Δ*f* offers the advantage of eliminating concentration as an explicit parameter. Also, the absolute slope and changes in the slope in the plots provide information about the kinetic regimes and conformational changes.[22,30,31] *D*−*f* plots of α-La I, Cyt *c*, BSA, and Mb revealed either just random

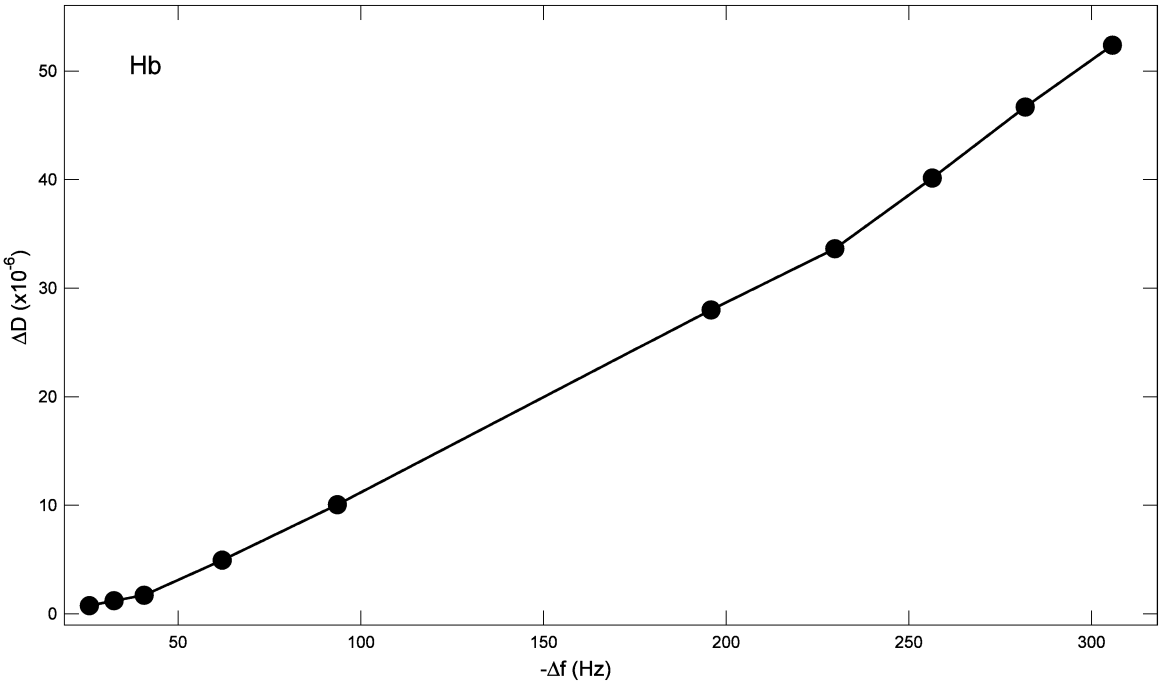

Figure 4. *D*−*f* plot for the sequential adsorption of Hb at 25 °C.

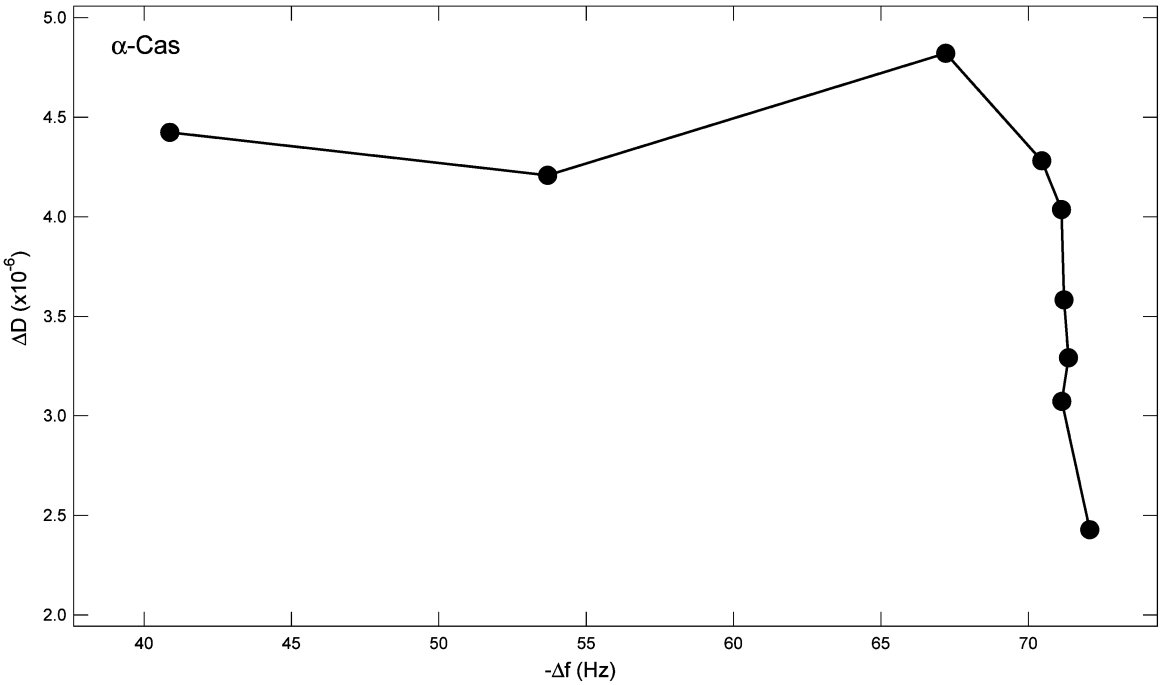

Figure 5. *D*−*f* plot for the sequential adsorption of α-Cas at 25 °C.

scatter or a first-order linear relationship throughout the data set, indicating that no significant changes in the structure of the adsorbed layer occurred throughout the experiment for these proteins (data not shown). From the *D*−*f* plots of α-La III and Lyz (Figure 3) it can be seen that both proteins display two linear regimes of significantly different slopes with the initial part having a smaller slope and the second one being significantly larger. This trend is more pronounced for Lyz. For α-La III, the breakpoint (Δf_B) occurs at ∼8 Hz, while for Lyz, the breakpoint occurs at ∼3 Hz. In the case of Hb, three linear regimes can be clearly distinguished (Figure 4) with breakpoints occurring at $\Delta f_{B1} \approx 50$ Hz and $\Delta f_{B2} \approx 230$ Hz. Identifying the regimes as I ($\Delta f < \Delta f_{B1}$), II ($\Delta f_{B1} < \Delta f < \Delta f_{B2}$), and III ($\Delta f > \Delta f_{B2}$) the slopes can be ranked as I < II < III. As shown in Figure 5, the *D*−*f* plot of α-Cas also contains two linear regimes with a breakpoint occurring at ∼67 Hz. However, the two regimes displayed by α-Cas appear to be different from those of α-La III, Lyz, and Hb in that the linear regime after the breakpoint has a steep negative slope.

Direct Deposition of Proteins. Normalized frequency shifts (of the third harmonic of the fundamental frequency) as time-dependent functions at 37 °C are shown in Figures 6 and 7 for the proteins studied here. As was the case for the sequential deposition method, all proteins studied here (with the exception of Hb) only displayed a single saturation plateau, indicating that adsorption did not proceed beyond monolayer coverage. Subsequent rinsing with buffer (10 mM citrate) and H_2O did not induce significant frequency or dissipation changes, which is

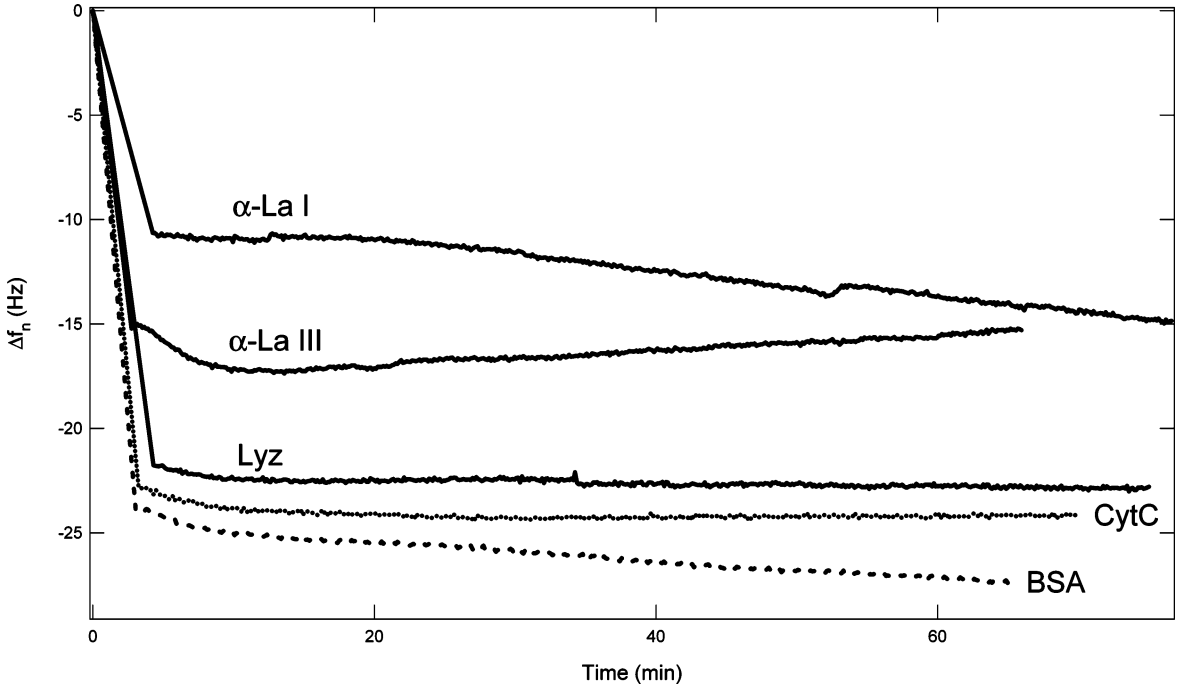

Figure 6. Changes in frequency acquired at the third harmonic as a function of time during direct adsorption of α-La I, α-La III, Lyz, Cyt *c*, and BSA at 37 °C.

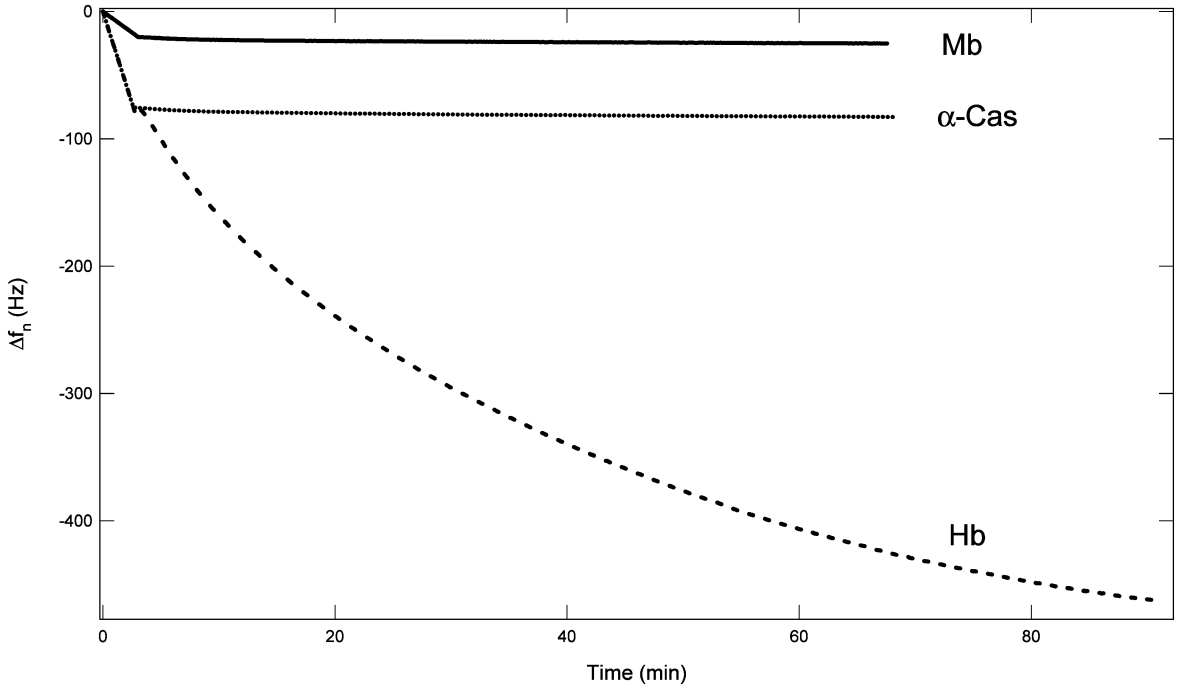

Figure 7. Changes in frequency acquired at the third harmonic as a function of time during direct adsorption of Mb, Hb, and α-Cas at 37 °C.

consistent with irreversible adsorption. As can be seen from Figures 6 and 7, all the proteins studied here with the exception of Hb have approached an equilibrium frequency shift within 5 min following addition of solute. For Lyz, Cyt *c*, Mb, and α-Cas, the frequency is constant following the initial shift. In the case of Hb, the system does not reach a stable equilibrium even after 20 h (isotherm not shown). α-La I and BSA appear to display a bimodal frequency shift — following the initial rapid frequency reduction, the frequency is slowly reduced further with the time constant approaching the time-dependent frequency resolution of the instrument. Conversely, α-La III appears to display a secondary minimum in the frequency shift prior to approaching equilibrium. Collected and calculated protein adsorption data using the direct deposition method at different temperatures are listed in Table 2. In general, the direct deposition method yields larger frequency shifts and thus higher surface coverages than the sequential deposition method at 25 °C, which is consistent with what has been reported by Brewer et al.[4] Listing the normalized frequency shifts at maximum surface coverage (Δf_{max}) at 25 °C in increasing order the proteins can be ranked as α-La I (∼15 Hz) < α-La III < Cyt *c* < Mb ≤ Lyz ≤ BSA < α-Cas ≪ Hb (∼534 Hz). Here it should be noted that Hb was allowed to equilibrate for a much longer time (20 h) at 25 °C than the other proteins (∼2 h) in an attempt to reach adsorption equilibrium. Comparing the ranked frequency shifts of direct deposition at 25 °C with those from the sequential

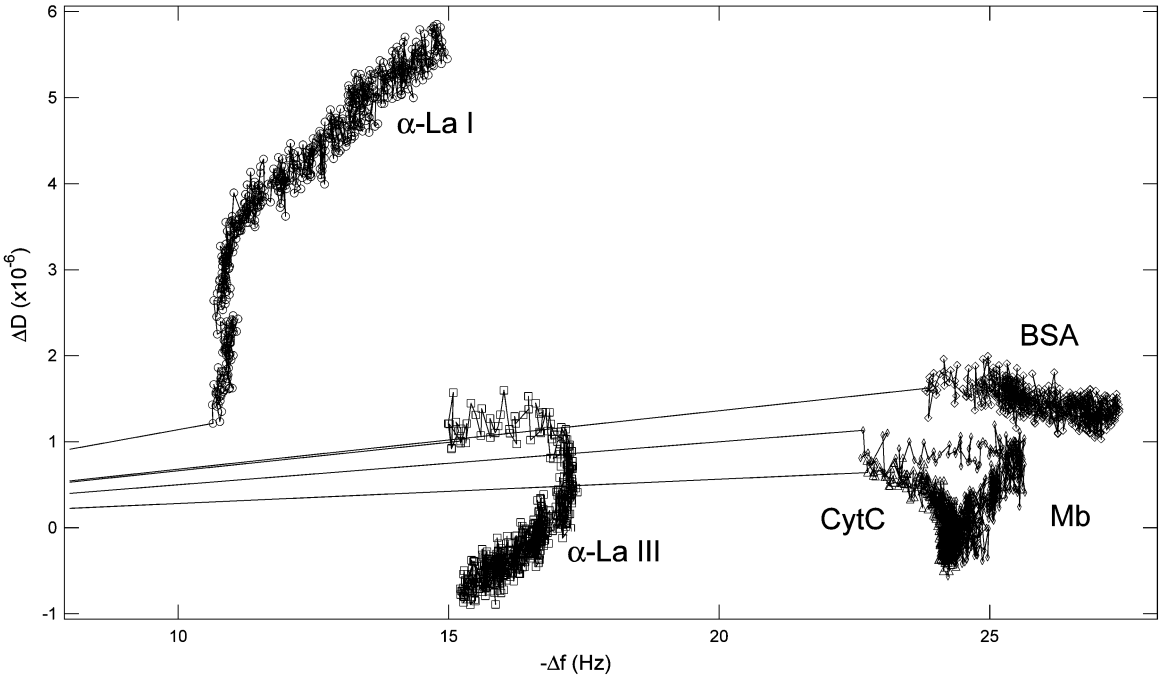

Figure 8. *D*−*f* plot for the direct adsorption of α-La I, α-La III, Cyt *c*, BSA, and Mb at 37 °C. Note that the density of data points (equispaced in time) becomes smaller the faster the kinetics in this type of plot. This explains the small number of points near the origin, where the kinetics is fast.

deposition method, it is apparent that the overall trend remains, albeit with some notable differences. Using the sequential deposition method, Lyz yields the smallest frequency shift; however, using the direct deposition method, Lyz causes a much larger Δf_{max}. Also, it is notable that using the direct deposition method, the ranking of α-La I and α-La III is opposite compared to the results obtained from the sequential deposition method. At 37 °C this order remains more or less constant with Lyz and Cyt *c* changing places in the ranked frequency shifts (Tables 1 and 2).

Ranking the $|\Delta D/\Delta f_{max}|$ ratios in increasing order for the direct deposition data at 25 °C (Table 2), the flexibility of the protein adlayers increases as Lyz < Cyt *c* < Mb < BSA < α-La I < α-Cas < α-La III < Hb. At 37 °C there are some notable changes to this trend, namely, that α-La I and α-La III change places, with α-La I forming a more flexible layer than Hb, yielding a $|\Delta D/\Delta f_{max}|$ order of Lyz ≪ Cyt *c* < Mb < BSA ≤ α-La III < α-Cas ≪ Hb ≪ α-La I. *D*−*f* plots of α-La I, α-La III, Cyt *c*, BSA at 37 °C and Mb at 50 °C are shown in Figure 8. All data sets are extrapolated to zero frequency and dissipation shifts, which marks the onset of protein adsorption. The lack of data points in the region immediately following addition of protein can be ascribed to the fast kinetics of the initial adsorption. α-La I displays two linear regimes with a breakpoint at ∼12 Hz with the first linear regime having a significantly steeper slope than the second. Two linear regimes can also be observed for Cyt *c* and BSA at 37 °C. Cyt *c* first displays a linear regime with a slightly negative slope followed by a linear regime with a steep negative slope (breakpoint ∼23 Hz). The first linear regime of BSA has a small, positive slope followed by a linear region with a moderately negative slope (breakpoint ∼25 Hz). α-La III (at 37 °C) and Mb (at 50 °C) each exhibit a region with a small positive slope followed by an inverted region (breakpoints at ∼17 and ∼26 Hz, respectively). *D*−*f* plots of α-La I, α-La III, Cyt *c*, and BSA and Mb at 25 °C and Lyz at 25 and 37 °C revealed either just random scatter or a first-order linear relationship throughout the data set, indicating that no significant changes in the structure of the adsorbed layer occurred throughout the experiment for these proteins (data not shown).

Figure 9 shows *D*−*f* plots of Hb at 25 and 37 °C. The *D*−*f* plot of direct deposition of Hb at 25 °C overlaps the corresponding plot from the sequential deposition exactly (described above); however; it also reveals one or two additional regimes above 400 Hz. Again it should be noted that the adsorption was allowed to go on for 20 h for this sample. Direct deposition of Hb at 37 °C shows the same general trend as for 25 °C but with a smaller slope above 200 Hz. *D*−*f* plots of α-Cas at 20, 25, and 37 °C are shown in Figure 10. Here, it can be seen that at 20 °C α-Cas displays the same general trend as α-La III (at 37 °C) and Mb (at 50 °C) with a linear regime followed by an inverted region (breakpoint ∼68 Hz). At 25 °C only a first-order distorted linear region can be seen, whereas at 37 °C α-Cas follows the same trend as BSA and Cyt *c* at the same temperature with two linear regimes—one with a small positive slope followed by a linear regime with a moderate negative slope (breakpoint ∼78 Hz).

Calculation of Binding Constants Using the Langmuir Model. Using data from the sequential deposition method and the Langmuir isotherm model the binding constants for the different proteins were calculated (Table 1). We apply the Langmuir isotherm model in this study with the understanding that most of the assumptions underlying this model are not satisfied for typical protein adsorption processes.[32] The Langmuir model assumes adsorption to occur on discrete sites and be reversible and interactions among sites to be negligible. For example, in the case of protein adsorption, the adsorbate molecules are so much larger than the surface lattice dimensions that the adsorbent is more reasonably considered to be a continuum than comprised of discrete sites. As such, we have not used the binding constants for approximation of the Gibbs free energy of adsorption ΔG_{ads} from the ascending adsorption isotherm (from $\Delta G_{ads} = -RT \ln K$). Rather, as the binding constant K is proportional to the ratio of adsorption and desorption rate constants ($K = k_a/k_d$), we use this value qualitatively as a measure of the surface affinity for each protein.

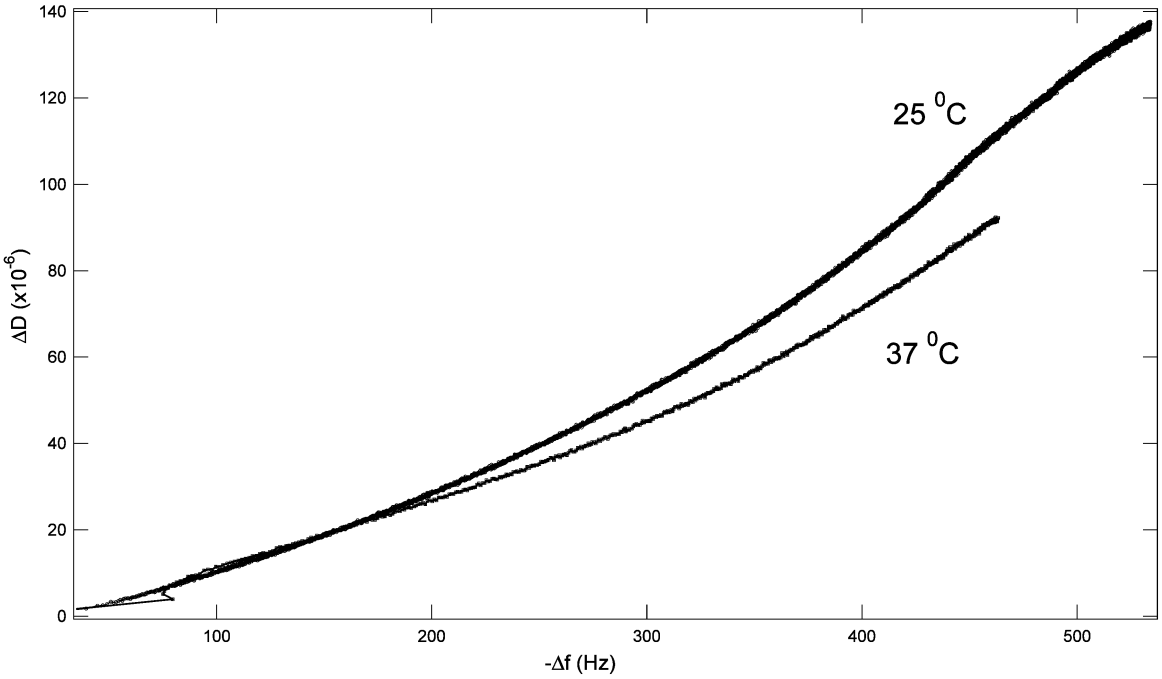

Figure 9. *D*−*f* plot for the direct adsorption of Hb at 25 and 37 °C. See also the legend of Figure 8.

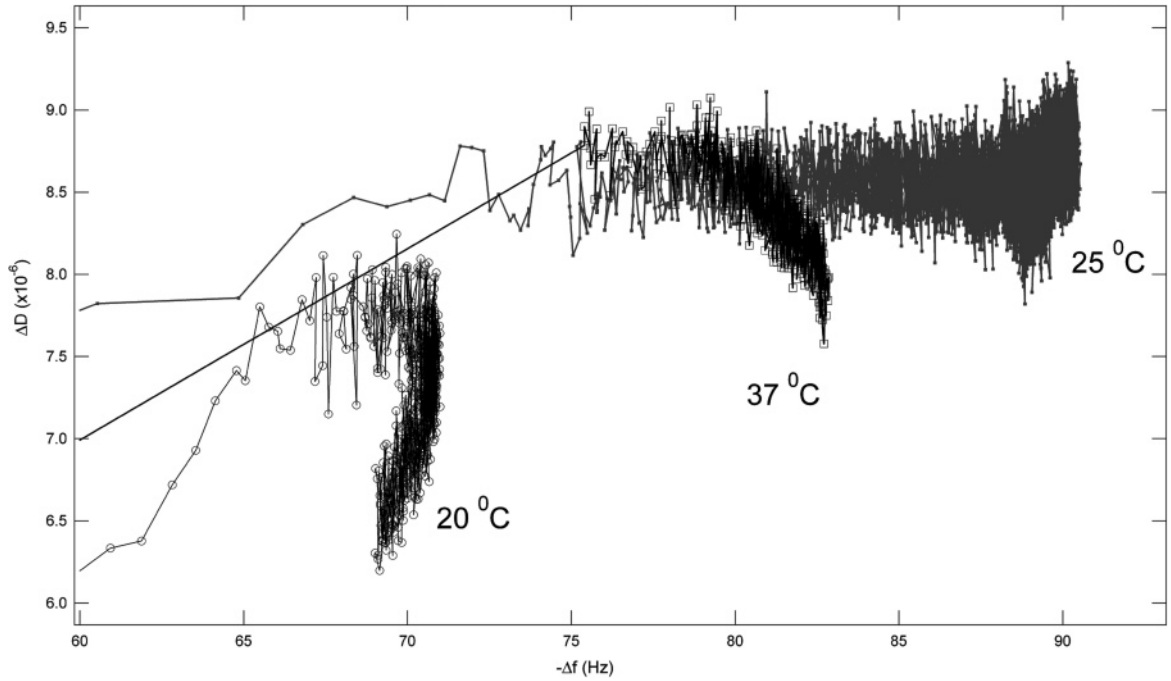

Figure 10. *D*−*f* plot for the direct adsorption of α-Cas at 20, 25, and 37 °C. See also the legend of Figure 8.

Moreover, we are aware that the value of the binding constant is affected by the deposition method with the direct method yielding significantly larger binding constants than the sequential deposition method for BSA onto citrate-coated Au.[4] However, we assume that the ranking of the surface affinities applies for the proteins studied here irrespective of deposition method as the differences between deposition methods are mostly related to other factors, as discussed below.

Bulk Protein Near- and Far-UV CD Temperature Scans. In order to investigate if conformational and stability factors could affect the deposition characteristics for each protein, we performed CD. Secondary structures for proteins in solution were assessed as a function of temperature using far-UV CD spectroscopy at 222 nm, a wavelength that is dominated by α-helical signal.[27] T_m values (melting temperatures) for transitions corresponding to 222 nm are shown in Table 3. Most proteins show clear transitions (Figure 11), where the majority of the change in ellipticity occurs within a temperature interval of 20 °C. Thus, for these proteins the first derivative of the ellipticity vs temperature function shows a clear, well-resolved peak. However, for α-La I, α-La III, and α-Cas there are no clear transitions. Excluding α-La I, III, and α-Cas, T_m values can be ranked as Hb < BSA < Lyz < Mb < Cyt *c*. Mean residue ellipticity at 25 °C can be ranked as Mb < α-La I < Cyt *c* < α-Cas < α-La III < Lyz < BSA < Hb.

Near-UV CD temperature scans can be used to probe the optical environment of tryptophans and other aromatic chromophores as a function of temperature. Neither α-Cas nor Mb showed a signal in the near-UV range. The remaining proteins showed well-resolved peaks in their first derivative, although

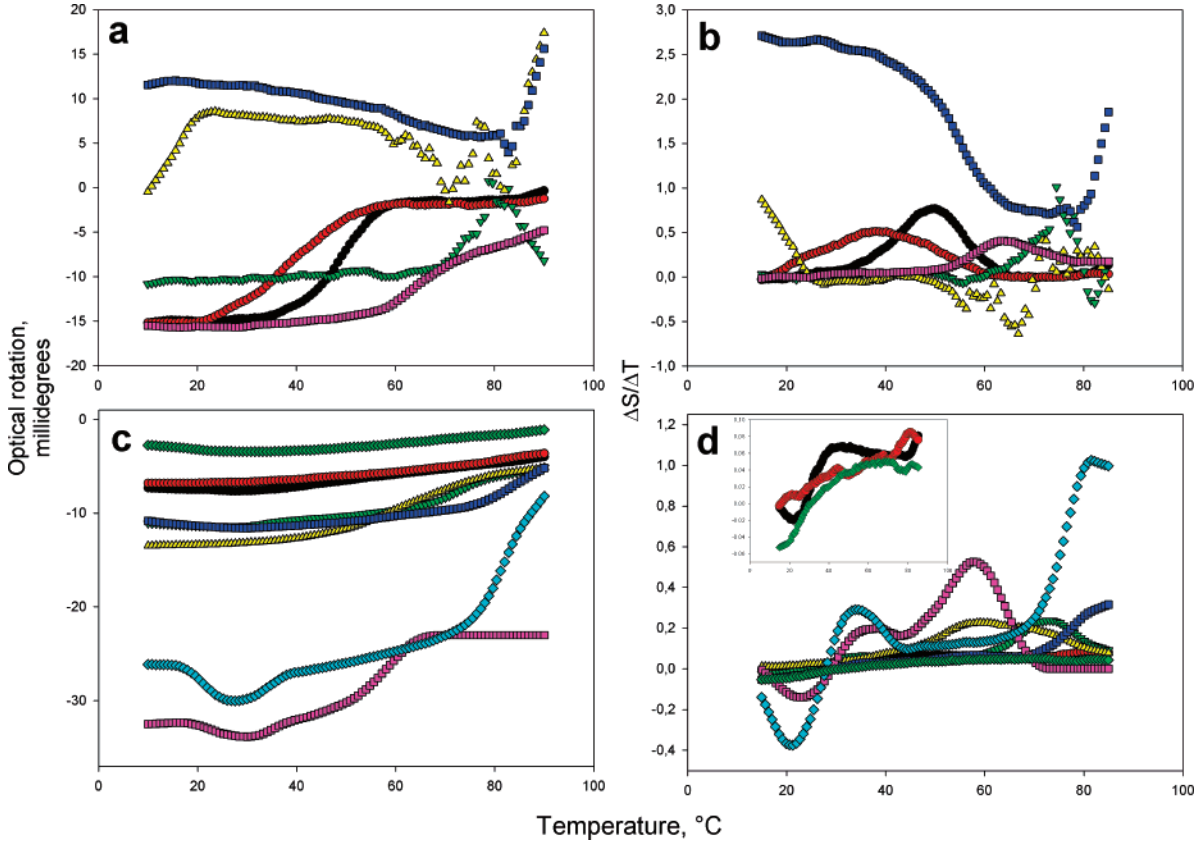

Figure 11. Near-UV (a) and far-UV (c) CD fixed wavelength temperature scan data. The former were acquired at wavelengths corresponding to the maximum signal for a given protein, typically in the 265−271 nm interval. The latter were acquired at 222 nm for all proteins. Corresponding first derivatives of the temperature scan curves are plotted in b for near UV data and d for far UV data. Briefly, the first derivative was calculated as $\Delta s/\Delta T = (s_2 - s_1)/(T_2 - T_1)$, where s is the dichroism signal and T is the temperature. Subscripts 1 and 2 refer to measurement points at temperature T and $T + 10$ °C, respectively. The first derivative was plotted against $(T_1 + T_2)/2$. Traces represent α-La I (black dot), α-La III (red dot), Hb (yellow triangle), Lyz (green upside down triangle), Cyt *c* (blue square), BSA (purple square), Mb (light blue diamond), and α-Cas (green diamond). Inset in d provides auxiliary view of α-La I (black dot), α-La III (red dot), and α-Cas (green diamond) proteins showing no clear transitions.

Hb, Cyt *c*, and Lyz showed random scatter in the CD spectra at higher temperatures, indicating onset of precipitation. This started at temperatures of 60, 82, and 78 °C for Hb, Cyt *c*, and Lyz, respectively, which caused added uncertainties in determination of T_m for these proteins. The values given in Table 3 are lower values. For the most part, tertiary structure T_ms coincide within a few °C with the corresponding value for secondary structure. α-La I and III tertiary structures have low stabilities, − 49 and 38 °C, respectively. Their transitions for secondary structure are unresolved according to the first derivatives of far-UV CD temperature scan data. The lack of robust secondary structure transitions and low tertiary structural stability is notable, especially when compared to the homologous Lyz. Ranking thermostability with respect to tertiary structure — this time including α-La I and III and excluding Mb and α-Cas — gives α-La III < α-La I < Hb < BSA < Cyt *c* ≈ Lyz.

On the basis of both near- and far-UV CD-monitored thermal stability data the proteins can, in order of increasing stability, be ranked as α-La III < α-La I < Hb < BSA < Lyz ≈ Mb ≈ Cyt *c*.

Discussion

In this study, the interaction between a small library of eight proteins and a model anionic surface has been investigated. Very briefly, the proteins employed here can be described as follows. α-La and Lyz are homologous proteins with very similar tertiary structures and primary sequence identities of approximately 35%.[33−35] Apart from biological function, the proteins differ in folding properties and calcium binding properties. Notably, α-La has the ability to form a stable molten globule[12] and strongly bind Ca^{2+},[36] while no such stable state or metal binding is reported for (hen egg white) Lyz.

The homologous Mb and Hb are heme-binding proteins involved in oxygen carrying and can be found in muscle and blood cells, respectively. While Mb is monomeric, Hb is tetrameric, consisting of a α and β subunit arranged in a $\alpha_2\beta_2$ quaternary structure. Mb is known to form a stable molten globule state in the absence of its heme group at moderately low pH values.[37]

Cyt *c* shuttles electrons between the two membrane-associated protein complexes cytochrome *c* reductase and cytochrome *c* oxidase on the inside of the inner mitochondrial membrane and is a part of the mitochondrial production of ATP. Cyt *c* molten globules have been stabilized both at electrodes set up to mimic the in vivo redox reaction,[38] in association with negatively charged membranes, and in bulk solution.[39−43]

α-Casein occurs in milk and probably has chelating and nutritional functions as well as providing stabilization and solubilization of other milk components. Its apparent size seems very dependent on conditions; it has little or no tertiary structure and the ability to form association/multimeric structures.[44,45] α-Cas has been described as a 'native molten globule' with a very high amount of conformational flexibility.[46]

BSA is a larger protein of 583 amino acids and is much studied as an important constituent of blood. (Bovine) Serum

TABLE 4: Molecular Properties of the Proteins Used in This Study[a]

protein	molecular weight (kDa)	dimensions (nm)	pI	overall charge[b]	thermal stability,[d] T_m, °C	ref[e]
α-La I	14.2	4.3 × 3.0 × 2.6	4.5	−7.3[c]	64.3	A, B, I
α-La III	14.2	4.3 × 3.0 × 2.6	4.5	−7.1	28.2	A, B, I
Lyz	14.3	4.4 × 3.2 × 2.4	10.5	7.9	74.0	A, K
Cyt *c*	12.4	3.7 × 2.5 × 2.5	10.1	7.3	77.0	A, C, D, L
BSA	67.0	9.0 × 5.5 × 5.5	4.8	−18.0	62.5	E, J
BSA	67.0	14.0 × 4.0 × 4.0	4.7−4.9	−18.0	62.5	C, F, G, J
Mb	17.2	4.5 × 3.5 × 2.5	6.8−7.0	−0.4	80.3	A, C, J
Hb	64.0	6.5 × 5.5 × 5.0	6.8−7.0	1.2		A, C
α-Cas	25.0	N/A	4.6	−12.4		H

[a] Under the experimental conditions studied here; pH = 8.55. [b] Charge as determined from titration curve using ExPASy proteomics tools (http://au.expasy.org/tools/). [c] Charge determined by Tanford−Kirkwood analysis (unpublished data). [d] Differential scanning calorimetry data from literature; it should be noted that entries correspond to various pHs and conditions. [e] Literature references for the protein dimensions and isoelectric points listed here. (A) Brookhaven protein data bank. (B) *Colloids Surf.* **1992**, *66*, 73−80. (C) Reference 14. (D) *Langmuir* **2004**, 20, 5879−5884. (E) *Langmuir* **2004**, *20*, 10055−10061. (F) *J. Am. Chem. Soc.* **2006**, *128*, 1939−1945. (G) *Adv. Protein Chem.* **1985**, *37*, 161−165. (H) From Sigma data sheet. (I) *Biochemistry* **1994**, *33*, 1889−1899. (J) *Toxicol. Lett.* **1998**, *100−101*, 387−391. (K) *Biochemistry* **1992**, *31*, 5278−83. (L) *J. Biochem. (Tokyo)* **2003**, *133*, 93−102.

albumin is a carrier protein responsible for transporting thyroid and fat-soluble hormones via the bloodstream.[47] Other physiological functions include control of serum osmotic pressure and pH buffering.[48]

By keeping the surface and solution conditions constant (10 mM citrate, pH = 8.55), we studied adsorption of these proteins with respect to deposition method (sequential or direct), overall protein charge (as determined by the pI, see Table 4 for an overview), and conformational flexibility of the adsorbates. The effect of temperature was also studied; however, we were not able to extract any robust trends from our dataset, and thus, temperature data are not discussed as a separate variable, only presented in Tables 1−2.

We consider two hypotheses for the interaction between the proteins and a citrate-coated Au surface as described by Brewer[4] et al. — an electrostatic binding hypothesis and a displacement hypothesis. The electrostatic binding hypothesis states that the attraction between the positive surface residues of the protein and the negative charge from the citrate are responsible for binding of the protein to citrate-coated Au surfaces. Here, it is assumed that the protein attaches itself to the passivating layer, i.e., the preadsorbed layer of citrate, on the gold surface without significant direct protein−gold interactions. The displacement hypothesis requires citrate to be displaced by the protein upon adsorption with amino acids (functional groups) such as lysine (amine), histidine (imidazole), or cysteine (thiol) interacting directly with the gold surface. Gold atoms at the surface are coordinately unsaturated, i.e., unoccupied orbitals are available for nucleophiles to donate electrons. As shown by Brust[49] et al., stronger electron donors such as amines, isothiocyanates, and alkanethiols are capable of displacing citrate from colloidal gold surfaces. Structural changes — including spreading — in the protein as a result of adsorption can lower the free energy of the system. The structural changes could be the result of denaturation on the surface while the protein displaces the citrate stabilizer. Consequently, the displacement hypothesis can be divided into two possible outcomes: displacement by the protein in its native structure or denaturation of the protein on the surface. Should denaturation occur during displacement, then the protein unfolds near the surface, exposing hydrophobic residues and presenting specific functional groups which interact with the gold surface. Dispersive and van der Waals forces must play some role in the above mechanisms as well. Brewer[4] et al. showed using QCM-D and ζ-potential measurements that BSA is associated with surface-bound citrate above pH 7 and that the *dominant* association of BSA with citrate-coated Au surfaces is electrostatic with BSA forming stronger ionic interactions,

SCHEME 1: Illustration of the Proposed Mechanism for Sequential Adsorption of α-La III and Lyz[a]

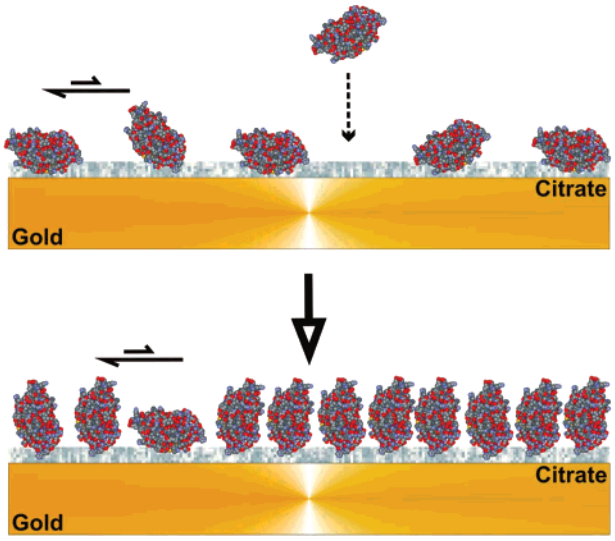

[a] Solid arrows depict equilibrium between two arbitrary protein orientations. The dashed arrow represents the initial adsorption of the protein. In order to accommodate more incoming proteins, the adsorbed molecules reorient to lower the average area needed per molecule. This will cause QCM plots ($D-f$) to display two distinct regimes, reflecting the different packing on the surface.

e.g., salt bridge formation, between the negatively charged carbonyl groups of citrate and the positively charged amine groups of the ∼60 lysines of BSA without any displacement of citrate. For adsorption of BSA onto a bare Au surface, the spreading/denaturation hypothesis is the most likely scenario.

Effect of Deposition Method on Protein Adsorption and Adlayer Characteristics. As stated in the Results section, direct deposition generally resulted in higher surface coverage than sequential deposition. Differences in surface coverage and adlayer structure from using either the sequential or the direct deposition method[4] can be understood from (a) adsorption kinetics and (b) protein−protein interactions (Schemes 1−3). During formation of an adsorbed layer on a surface each adsorbing macromolecule passes through the following steps: (1) transport toward the surface, (2) attachment to the surface, and (3) reorientation/spreading.[14] The degree to which the proteins will be able to reorient and/or spread on a surface in order to maximize favorable interactions will depend on the conformational flexibility of the protein, which will be discussed later. Let τ_d = the time required to transport molecules toward

SCHEME 2: Illustration of the Proposed Mechanism for Direct Adsorption of α-La I[a]

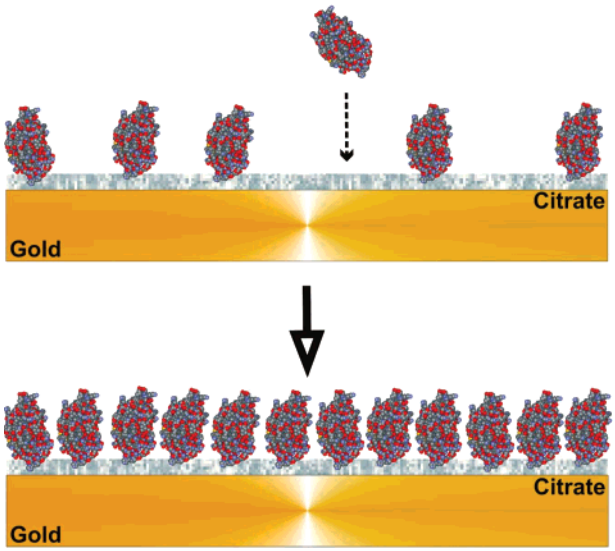

[a] The dashed arrow represents the initial adsorption, wherein the approaching adsorbates only experience protein−surface interactions. As the surface coverage increases, the approaching adsorbates also experience protein−protein interactions, which can be observed as two distinct regimes in the $D-f$ Plots. The second regime (where protein−protein interactions are included) is characterized by a lower slope, corresponding to a lower adsorption rate.

and deposit them on the surface and τ_s = the time required for the molecules to reorient/spread on the surface. Generally, if $\tau_d > \tau_s$, each adsorbing molecule can reorient and/or spread before it is surrounded by other molecules, resulting in low surface coverage and a thin adsorbed layer. Conversely, if $\tau_d < \tau_s$, the molecules are enclosed by neighbors before they have time to reorient/spread, yielding higher surface coverage and potentially a thicker adsorbed layer. For the same protein adsorbing to the same surface, τ_s will be the same irrespective of deposition method; however, τ_d will most likely be different. More specifically, in the sequential deposition method, adsorption starts out at low protein concentrations and thus a lower adsorbate−surface collision probability, meaning a higher τ_d value. In the direct deposition method, the protein concentration is high, yielding a much higher collision probability and thus a low τ_d value. Consequently, it is to be expected that direct deposition results in higher surface coverages than the sequential deposition method, which is supported by the general trend in this data set. This is also supported by the modeled layer thicknesses for sequential and direct deposition at 25 °C; as can be seen from Tables 1 and 2, direct deposition yields thicker layers for five out of eight proteins. In the case of α-La I and Mb, the layer thickness is independent of deposition method, while for Cyt *c*, sequential deposition yields a thicker adsorbed layer than direct deposition. Here, it should be noted that the ability to change orientation on the surface will depend both on the preferred number of contact points between protein and surface and on the conformational flexibility of each protein, as discussed later.

Further information about kinetic regimes and surface-induced conformational changes for the proteins studied here can be found in the $D-f$ plots for sequential (Figures 3−5) and direct (Figures 8−10) deposition. It is apparent that the deposition method greatly affects the conformation of the adsorbed layers in that many of the proteins display different $D-f$ behaviors and thus different adlayer characteristics (depending on the deposition method). For the proteins which do not form

SCHEME 3: Illustration of the Proposed Mechanism for Direct Adsorption of α-La III[a]

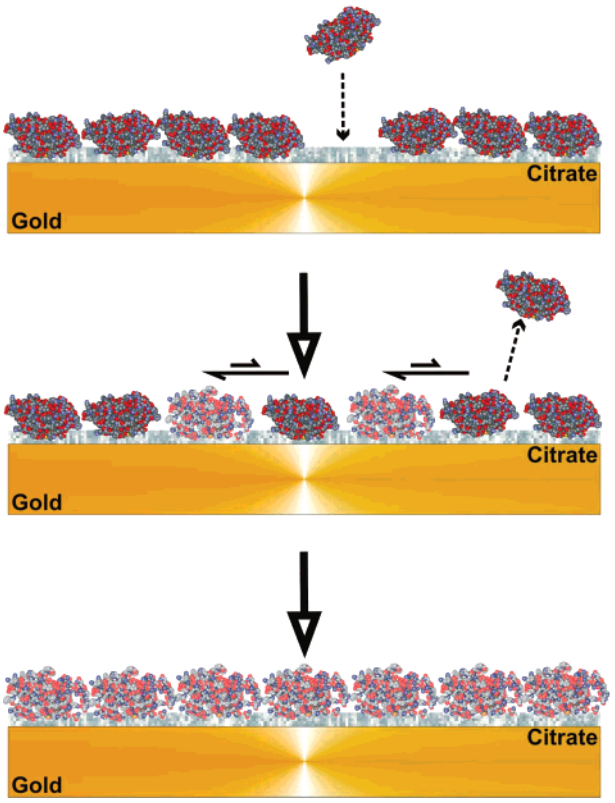

[a] The protein initially adsorbs in higher amounts than what can be optimally accommodated on the surface. Hence, as the protein spreads and adopts an equilibrium conformation, the required area per molecule increases, leading to desorption of "surplus" proteins and release of trapped water until an apparent equilibrium is reached. This can be observed as an "inversion" in the $D-f$ plot.

multilayers/supramolecular assemblies, three types of adsorption behavior could be distinguished outside of simple one-state behavior, i.e., where the $D-f$ plots either show no breakpoints or consist of random scatter.

(1) Concentration-dependent conformation/orientation changes. Sequential adsorption of Lyz shows two distinct linear regimes with the initial part having a smaller slope and the second one being significantly larger (Figure 3). This type of behavior can also be seen for sequential deposition of α-La III and adsorption of Hb, as discussed later. However, in light of Lyz and α-La III not displaying multilayer formation, our interpretation is that the surface-bound proteins experience a conformational/orientational change upon increasing the bulk concentration.[30,31] In order to accommodate incoming proteins the adsorbed molecules adopt a more outstretched conformation, possibly reducing the number of binding sites per protein (Scheme 1). A $D-f$ plot for direct deposition of Lyz (data not shown) only displayed random scatter around a single, first-order linear regime, indicating that no conformational changes occurred during formation of an adsorbed layer. Comparing the induced energy losses per coupled unit mass at maximum coverage ($|\Delta D/\Delta f_{max}|$, see Tables 1−2) for the two methods also shows that in the case of Lyz direct deposition yields a significantly more rigid layer than sequential deposition. Also, the modeled layer thickness for sequential deposition of Lyz (1.2 nm, Table 1) is much lower than for direct deposition (5.5 nm, Table 2) and indeed the lowest for the entire dataset. Here it should be kept in mind that the modeled thickness is averaged over the entire surface, and an incomplete monolayer or any open spots would

thus cause an underestimation of the layer thickness, as is probably the case for sequentially deposited Lyz. Moreover, for Lyz, direct deposition also yields a higher surface coverage than for sequential adsorption without any detectable conformational changes, which is consistent with a tighter packing of molecules with a similar conformation/orientation. The observation that sequential deposition results in a more flexible adlayer at lower surface coverage than what was found for direct deposition could emanate from surface-induced conformational changes (i.e., partial unfolding) or unfavorable protein−protein interactions. In light of Lyz behaving as a rigid protein with no stable folding intermediates, the latter is more likely.

(2) Random sequential adsorption. Sequential deposition of α-La I displays a simple one-state behavior (data not shown) which indicates the absence of concentration-dependent conformational changes. However, the $D-f$ plot indicates a bimodal adsorption behavior for the direct deposition of α-La I, which can also be seen from the adsorption isotherm (Figures 6 and 8). The $D-f$ plot (Figure 8) displays two linear regimes with the opposite trend of what was found for Lyz; the slope of the second regime is significantly lower than for the first. We interpret this as random sequential adsorption in which vacant adsorption sites are filled at lower rates proportional to increased surface coverage (Scheme 2). Comparing $|\Delta D/\Delta f_{max}|$ values and modeled thicknesses for sequential and direct deposition of α-La I reveals that direct deposition yields a significantly more flexible layer, albeit with a similar mean thickness as for sequential deposition.

(3) Surface-induced spreading/conformational changes. α-La III also displays different adsorption behavior between deposition methods, as shown in Figures 3 (sequential deposition) and 8 (direct deposition). Sequential deposition of α-La III appears to follow a similar trend as that discussed for sequential deposition of Lyz (albeit without as marked a transition between the linear regimes); however, direct deposition promotes a quite different behavior (Figures 6 and 8). From the adsorption isotherm (Figure 6) a minimum in the frequency shift can be observed prior to leveling off toward an apparent equilibrium, which indicates that some of the initially adsorbed protein is desorbed. This phenomenon can be observed as an "inversion" in the $D-f$ plot (Figure 8), where the inflection point marks the maximum frequency shift. We interpret these results as conformational changes/spreading on the surface, as illustrated in Scheme 3. Here, the protein initially adsorbs in higher amounts than what can be optimally accommodated at the surface. Hence, as the protein adopts the equilibrium conformation, presumably including spreading, the area per molecule increases, leading to desorption of "surplus" molecules until an apparent equilibrium is reached at the surface. It should be mentioned that the observed frequency increase emanates from two sources: desorption of "surplus" protein as described above and release of trapped water upon spreading/adaptation of the remaining surface-bound proteins. This behavior was also observed for Mb, as can be seen from Figure 8.

Net Favorable Electrostatic Interactions Occur Regardless of Overall Protein Charge. In order to study the effect of the overall protein charge on adsorption, we employed a library of proteins with isoelectric points both above and below the solution pH used here (pH = 8.55), i.e., acidic and basic proteins, as listed in Table 4. Spontaneous adsorption of a protein to an interface is driven by an overall decrease in the Gibbs free energy (i.e., $\Delta G_{ads} = \Delta H_{ads} - T\Delta S_{ads} < 0$), with the affinity of the protein being reflected in the magnitude of the Gibbs energy reduction. On the basis of the observations that proteins have high affinities for solid/water interfaces and that protein adsorption to solid surfaces tends to be irreversible, it has been suggested that ΔG_{ads} is large (and negative) for most protein adsorption processes.[32] As noted in the Results, calculation of binding constants using the Langmuir model, we have not calculated the Gibb's free energy values associated to the protein surface binding constants. We employ the K values as a measure of surface affinity in that protein adsorption appears to be irreversible under these conditions.

Thus, from the calculated K values (Table 1) the surface affinities of the proteins in 10 mM citrate (pH = 8.55) at 25 °C can be listed as (in increasing order) $Mb^n < Cyt\ c^p < BSA^n < \alpha\text{-La III}^n < \alpha\text{-La I}^n \cong Lyz^p \ll \alpha\text{-Cas}^n$. The superscripts n and p refer to the isoelectric point (pI) of the protein (see Table 4) being below or above the solution conditions studied here (pH = 8.55), indicating an overall negative (n) or positive (p) charge, respectively. Hb is excluded from this ranking as the adsorption behavior of this protein does not conform to a Langmuir isotherm model due to multilayer formation (see, e.g., Höök[30] et al.). The adsorption isotherms of the other proteins yielded reasonable fits ($R^2 \geq 0.93$) to the Langmuir model. As can be seen from the ranking of surface affinities above, there is no apparent correlation between the overall charge of the protein (as determined by the pI) and the affinity toward the surface for the proteins and surface studied here. Hence, from our data the adsorption does not seem to be driven by global electrostatic effects. This is in agreement with the findings reported by Brewer et al.[4] We therefore propose that favorable electrostatic interactions may occur regardless of the overall charge of the protein, where citrate interacts with positively charged surface groups or domains on the proteins. Thus, the detailed distribution of charges on the protein before and after adsorption is of more importance than overall protein charge in solution. It should be noted that protein ability to adopt an asymmetric charge distribution at the surface will depend on protein size (molecular weight) as well as the conformational flexibility, with larger and/or more flexible globular proteins (e.g., BSA) being more prone to surface-induced conformational changes. Asymmetric charge distribution on the surface of a protein can affect its adsorption behavior in at least two ways. First, interactions between the aqueous adsorbent interface and a highly charged region on the protein surface can result in oriented protein adsorption. For instance, the protein will tend to adsorb with the region oriented surface-wards if the region and adsorbent are oppositely charged. Second, asymmetric charge distributions will influence a protein's permanent dipole moment. With optimal protein orientation, the bulk of the protein and its local positive charges will shield unfavorable Coulombic interactions between negatively charged residues and the surface. For globular proteins the dipole moments are usually large[50] with α-helices, β-sheets, and fixed surface charges all making substantial contributions to their values.[32,51]

Adsorption Onto a Surface May Induce Formation of Supramolecular Structures. Two of the proteins studied here — hemoglobin (Hb) and α-casein (α-Cas) — have the ability to form supramolecular structures at interfaces. The heme-binding protein Hb is involved in carrying oxygen and found in muscle and blood cells. Hb is tetrameric, consisting of α and β subunits arranged in a $\alpha_2\beta_2$ quaternary structure, and is predominantly helical (Table 3). α-Casein occurs in milk and probably has chelating and nutritional functions as well as providing stabilization and solubilization of other milk components. Its apparent size seems very dependent on solution conditions; it has little or no tertiary structure and is capable of forming association/

multimeric structures/micelles in bulk.[44,45] α-Cas has been described as a 'native molten globule' with a very high amount of conformational flexibility.[46] These observations are supported by the CD results in this study, which show low mean residual optical rotation at 222 nm and no clear temperature transitions (Table 3).

Upon adsorption to solid interfaces, Hb is capable of forming multiple layers as a function of protein concentration, as observed earlier.[30] This observation can be rationalized by assuming that the Hb intrinsic ability to form quaternary structures is enhanced at the surface. This enhancement could be brought about by the increase of protein concentration at the surface combined with surface-mediated protein orientation, thus facilitating further association, orientation, and immobilization. In the case of Hb, sequential and direct deposition yield completely overlapping $D-f$ plots with respect to both slopes and breakpoints between linear regimes for the data collected at 25 °C (Figures 4 and 9). The first breakpoint corresponds well to that reported by Höök;[30] however, the concentration range used here exceeds that of earlier studies. From the modeled layer thickness of sequentially deposited Hb this transition from mono- to multilayer can also be seen quite clearly; the best fit was found for a film composed of one inner rigid layer (∼6.6 nm) and one peripheral viscoelastic layer (65.8 nm) at maximum recorded surface coverage (Table 1). As can be expected, Hb forms the most flexible adlayers of the proteins studied here regardless of deposition method.

Of the proteins examined in this study, α-Cas and Hb have in common that they both adsorb as viscoelastic films in a thickness exceeding native protein dimensions with at least a factor of 2. Thus, multiple layers of proteins are stabilized on the surface. Hb, as discussed above, forms successive layers of proteins, a process that in the case of direct deposition at 25 °C continued until the experiment was terminated at 20 h. In contrast, adsorption of α-Cas reaches a well-defined plateau for both deposition methods and all temperatures investigated here. α-Cas was also found to have the decidedly highest surface affinity of all proteins studied here — with the exception of Hb (Table 1). For sequential deposition of α-Cas the $D-f$ plot reveals a significant breakpoint at 67 Hz with a subsequent change in slope to be steeply negative (Figure 5). Since the CMC for α-Cas was found to occur approximately in the same concentration range as the breakpoint (∼3 μM), we interpret the breakpoint observed in Figure 5 as formation of α-Cas micelles at the surface. This is further supported by ΔD decreasing abruptly and significantly (approximately by a factor of 2, from $\sim 4.5 \times 10^{-6}$ to $\sim 2.2 \times 10^{-6}$) while remaining positive (i.e., no displacement of the passivating layer). Such an increase in order is consistent with a transition from single, flexible molecules to more organized structures such as micelles.

Comparing sequential and direct deposition of α-Cas at 25 °C there are several distinctive differences. First, direct deposition results in higher adsorbed amounts (82.6 vs 68.3 Hz, see Tables 1 and 2), which is in good agreement with the overall trend observed for the two deposition methods. Second, comparing the flexibilities of the adsorbed layers ($|\Delta D/\Delta f_{max}|$, Tables 1 and 2) for the two deposition methods shows that direct deposition yields an approximately twice as flexible (95.0×10^{-9} vs 43.2×10^{-9} Hz^{-1}) and twice as thick (∼30 vs ∼15 nm) adsorbed layer than sequential deposition. Last, while the $D-f$ plot of sequential deposition of α-Cas shows a marked breakpoint as discussed above, the $D-f$ plot of direct deposition does not show any significant changes in ΔD upon increased frequency shifts (Figure 10), indicating that no conformational changes or self-association occur during layer formation. This can be explained by the fact that for the direct deposition of α-Cas the concentration exceeds CMC by a factor of ∼10. Hence, α-Cas adsorbs in the form of micelles during direct deposition, whereas for sequential deposition the protein initially adsorbs in the form of monomers before self-assembling at the surface. Differences in adsorbed mass, layer flexibility, and film thickness can then be understood in terms of size differences between micelles formed in bulk and at the surface. As the energy barriers for surface-induced micelle formation/self-assembly is typically lower than for the equivalent micelle formation in bulk,[52] it is not unexpected that the micelles formed at the surface are significantly smaller, which is in agreement with what is observed here. Differences in adsorbed mass, layer flexibility and thickness, and $D-f$ behavior for direct deposition of α-Cas at 20 and 37 °C will not be discussed in detail in this study as they can probably be related to the temperature dependence of CMC for α-Cas, which was not studied here (see Table 2). Thus, for α-Cas, micellar size and adlayer rigidity can be tailored through choice of deposition method.

Hb and α-Cas together form examples of two types of surface behavior where large amounts of protein can be adsorbed. In both cases, the surface lowers the thermodynamic cost of assembly into larger structures. For Hb this is manifested as successive layers of multimers while for α-Cas in formation of micelles. As such, it appears that for both Hb and α-Cas adsorption onto the surface enhances tendencies to multimeric behavior already present in the proteins.

Protein Conformational Flexibility Facilitates Interaction with Surfaces. According to Haynes and Norde,[32] the entropic contributions (ΔS_{ads}) to the free energy of adsorption (ΔG_{ads}) is structural unfolding and rearrangement of protein hydration. In this discussion we will focus on rearrangements in the protein structure upon adsorption. Large positive ΔS_{ads} values can arise from unfolding — reversible or irreversible — of protein molecules upon adsorption. Creighton[51] estimated that the increased rotational freedom of the polypeptide backbone resulting from the complete unfolding of a native protein will lead to an entropy gain of 10−100 $J \cdot K^{-1} \cdot mol^{-1}$ of amino acid residue. There is much evidence coming from various experimental techniques that rearrangement of protein structure takes place upon interaction with a range of surfaces — including moderately hydrophobic polystyrene surfaces and sol−gel systems.[11,53−56] Also, there are numerous reports of proteins with low native-state stabilities that adsorb readily under seemingly unfavorable conditions where the surface is hydrophilic and/or the protein and adsorbent surface carry the same charge sign.[1,4,11,57] For six out of the eight proteins studied here (except Cyt *c* and Lyz) adsorption occurs on a hydrophilic adsorbent carrying the same charge sign as the overall charge of the protein.

While protein thermal stability is not the same as flexibility, the characteristics are related.[58] Also, protein ability to form stable intermediately folded states is expected to facilitate the rearrangement of protein on a surface, i.e., a protein which possesses a stable folding intermediate does not have to pay the full thermodynamical cost of complete unfolding to conform to a new environment at an interface. In light of this, our results on bulk structural stabilities (Bulk Protein Near- and far-UV CD Temperature Scans section, Table 3) can be seen to correlate inversely with direct deposition adlayer flexibilities (Direct Deposition of Proteins section).

$$\alpha\text{−Cas} < \alpha\text{−La III} < \alpha\text{−La I} < \text{Hb} < \text{BSA} < \text{Lyz} \approx \text{Mb} \approx \text{Cyt } c \text{ (Stability)}$$

Hb > α−La III > α−Cas > α−La I > BSA > Mb > Cyt *c* > Lyz (Adlayer flexibility)

α-Cas is given the lowest thermal stability in the sense that it has no thermal transitions at all; its structure is known to be loose and show little cooperativity even at room temperature.[44,46] Lyz, Mb, and Cyt *c* all showed similar and relatively high secondary and tertiary structural stability (secondary structure T_ms 73−81 °C and corresponding values in the near-UV range ≈ 80 °C, Table 3). However, in contrast to Lyz, Cyt *c* and Mb have the ability to form stable MG states,[37,39] which are states that are inherently flexible, since they lack fixed tertiary interaction.[12] Thus, we rationalize the Cyt *c* and Mb ability to form flexible adlayers to their ability to form MG-like conformations at nonbulk conditions. Similarly, we explain the very flexible layer that Hb forms from formation of multilayers, as discussed above. The fact that Hb forms more flexible layers than α-Cas can be explained by α-Cas self-assembling into micelles at the surface while Hb forms flexible multilayers. Relating *D*−*f* data directly to adsorbed protein conformational flexibility is complicated by the fact that *D*−*f* data does not distinguish between the flexibility of the protein folding state and the flexibility of the layer that stems from loose protein packing, rearrangement of protein orientation, and other interprotein phenomena. Moreover, relating protein bulk properties to their adlayer properties is made difficult by the fact that proteins that appear relatively rigid at bulk conditions may actually be quite easily unfolded. A case in point is the ease of which α-La I is unfolded by micromolar concentrations of SDS; at the same concentration the homologous Lyz is unperturbed.[59] A similar, less extreme case has been reported for Cyt *c*, where millimolar amounts of surfactant are required.[40]

Thus, a degree of flexibility in the protein structure — as opposed to a "hard", crystal-like protein with a comparatively high energetic barrier toward unfolding — would facilitate efficient protein binding. This scheme would fit well with other works on protein−membrane interactions where transitions to molten globule-like states are found to facilitate membrane interactions.[6,7,60] Similar observations have been made for proteins adsorbing to nanoparticles.[11] More generally, it has been proposed recently that protein order-to-disorder transitions and vice versa should be emphasized when accounting for a number of phenomena, among them intercalation of proteins into membranes.[61]

Cofactors Affect Binding through Limiting Conformational Flexibility. At bulk conditions, both Mb and Cyt *c* possess very stable helical structures, with Cyt *c* and Mb displaying T_m = 82 and 81 °C, respectively (Table 4). The Cyt *c* tertiary structure transition appears to coincide with the melting of the helices. Adsorbed to the Au−citrate surface they show similar surface coverage in proteins·cm^{-2} for sequential deposition (Table 1). Note that due to differences in molecular weights for Mb and Cyt *c* (17.2 and 12.4 kDa, respectively), the frequency shifts upon adsorption vary accordingly. Interestingly, the surface affinities for the two proteins are very similar, despite Mb being negatively charged and Cyt *c* being positively charged under the experimental conditions studied here (Table 1). It is tempting to explain the very similar adsorption characteristics with the loss or altered ligation of the heme group, although our results contain no direct information about its behavior. Loss or perturbation of the heme group is, however, associated with the molten globule state.

Conclusions

In this work we attempt to chart the interaction of a range of proteins with citrate-coated gold surfaces and relate our findings to protein charge and conformational stability and flexibility. We propose a generalization of protein−negatively charged surface interactions: (i) Net positive (opposite) charge is not necessary for efficient binding. Rather, it is very likely that local patches of positive charge, secondary structure configuration, as well as electrostatic shielding of negative charges by the body of the protein and its positive charges are the dominant contributions to the binding. (ii) The efficiency of the subsequent short-range consolidation of adsorption depends on protein ability to adapt its fold to take thermodynamic advantage of the interface environment. This step is facilitated by the protein having stable intermediates and/or being flexible in its native state. A surface that stabilizes partially unfolded conformations, either by the presence of surface adsorbates, the surface itself, or nonbulk conditions like suppressed solvent pH or dielectric constant, will favor tight interaction. (iii) Adsorption to a surface may enhance protein tendency to form higher-order structures, such as multilayers or micelles. This in turn leads to high amounts of protein adsorbed. (iv) The conformations favored at the interface will also depend on the nature of the interface. A fluid membrane might allow a protein to penetrate deeply into it, while a solid interface, such as a metallic surface, will favor spreading rather than penetration. The protein−surface interactions studied here most likely reside between these two extremes as the primary interaction is going to occur between protein and the passivating layer, but we cannot conclusively state that penetration into the citrate layer does not occur. (v) Lipid head groups or surface adsorbates are important for modulating interface electrostatics and determining to which degree the binding can be consolidated by hydrophobic interaction and hydrogen bonding. (vi) Adsorptive properties such as surface coverage, layer thickness, and adlayer flexibility are tunable through choice of deposition method.

Some of the points i−vi have been proposed by other authors in a variety of contexts and formulations. For instance, the emphasis on protein local charge as opposed to overall charge for the efficient interaction with lipid−water interfaces has been characterized at a detailed level for at least two systems.[60,62] The idea that the molten globule is important for proteins at interfaces (in this case lipid bilayer−water interfaces) was proposed by Bychkova et al. in 1988.[63] It has since then been used to rationalize a wide range of biological phenomena. Two examples among many are protein import into the mitochondria[64−66] and bacteriophage infection facilitated by viral coat proteins transferring to a molten globule state as they interact with the bacterial membrane.[67−70] The realization that conformational changes may be induced by nonbulk conditions at interfaces has been discussed by many authors, including Watts, Kinnunen, and Bychkova.[8,39,71] Thus, while points i−iv and vi have been applied in various forms to various systems, there exists—as far as the authors can establish — no work that has systematically elucidated a set of proteins at identical experimental conditions and discussed the findings in terms of these considerations. We suggest that points i−vi represent a fruitful (but not exhaustive) list of discussion points for works concerning protein−interface systems.

In this work we performed the experiments in a pH 8.55 citrate solution as this solved problems related to adlayer properties and colloid stability. The conditions are significantly more basic than physiological pHs, and it would of course be interesting to know how these protein−citrate−gold systems

behaved closer to pH 7.4. Hb and Mb would have an overall charge close to zero; some proteins exhibit heightened surface affinities at such conditions, likely due to no net repulsion between molecules adsorbed on the surface (Table 4). This might result in more rigid films, at least in the case of monolayers.

As stated in the Introduction, interaction of proteins with surfaces is of importance for designing materials suitable for bioimplants. Our protein matrix has shown a variety of responses to a citrate−Au surface. Protein accumulation at this surface would be low for proteins such as Lyz, i.e., proteins with low flexibility and inability to access folding intermediates. Conversely, flexible proteins with favorable dipole moments and ability to form layers or aggregates are expected to accumulate if exposed to an implant having this surface coating. Changing the surface to being weakly positive might form part of a strategy for reducing protein accumulation at bioimplant interfaces. Almost all studies of proteins that display an affinity for biomembranes report that the presence of negative charge enhances the interaction.[7,57,72−74] Since net charge and/or dipole moment very likely account for the initial association, it might be expected that there is a relationship between these characteristics and the rate of adsorption at very low protein concentrations when protein hydrodynamic radius is taken into account. However, as the surface becomes crowded other phenomena dominate. For instance, if a protein dipole associates with its positively charged side to a negatively charged interface, a protein adsorbing onto the same site can orient in the same manner. A protein with an overall positive charge might adsorb with another positive patch oriented toward incoming proteins. In such a situation the long-range ionic interaction important for the initial step would be quickly removed, hampering accumulation of protein at the surface. Thus, strategies for reducing protein adsorption might, in addition to taking protein flexibility into account, also include removing the cause of long-range Coulombic protein−protein and protein−interface interaction.

Abbreviations

α-La I, α-lactalbumin type I; α-La III, α-lactalbumin type III; BSA, bovine serum albumin; Hb, hemoglobin; Mb, myoglobin; Cyt *c*, cytochrome *c*; α-Cas, α-casein; Lyz, hen egg white lysozyme; QCM, quartz-crystal microbalance; MG, molten globule; CD, circular dichroism.

Acknowledgment. W.G. gratefully acknowledges support by NFR/NTNU grant 10287305, and Ø.H. acknowledges support from The Norwegian Cancer Society. W.G. and S.V. are grateful to Carl Marius Roel for assisting with QCM-D measurements. We thank Professor Aurora Martinez at the Department of Biomedicine, University of Bergen, for helpful discussions and careful proof reading.

References and Notes

(1) Norde, W.; Anusiem, A. C. I. *Colloids Surf.* **1992**, *66*, 73.
(2) Roach, P.; Farrar, D.; Perry, C. C. *J. Am. Chem. Soc.* **2005**, *127*, 8168.
(3) Roach, P.; Farrar, D.; Perry, C. C. *J. Am. Chem. Soc.* **2006**, *128*, 3939.
(4) Brewer, S. H.; Glomm, W. R.; Johnson, M. C.; Knag, M. K.; Franzen, S. *Langmuir* **2005**, *21*, 9303.
(5) Bertini, I.; Turano, P.; Vasos, P. R.; Bondon, A.; Chevance, S.; Simonneaux, G. *J. Mol. Biol.* **2004**, *336*, 489.
(6) Taneva, S. G.; Donchev, A. A.; Dimitrov, M. I.; Muga, A. *Biochim. Biophys. Acta-Biomembr.* **2000**, *1463*, 429.
(7) Banuelos, S.; Muga, A. *J. Biol. Chem.* **1995**, *270*, 29910.
(8) Kinnunen, P. K. J.; Koiv, A.; Lehtonen, J. Y. A.; Rytomaa, M.; Mustonen, P. *Chem. Phys. Lipids* **1994**, *73*, 181.
(9) Haynes, C. A.; Norde, W. *J. Colloid Interface Sci.* **1995**, *169*, 313.
(10) Billsten, P.; Freskgard, P. O.; Carlsson, U.; Jonsson, B. H.; Elwing, H. *FEBS Lett.* **1997**, *402*, 67.
(11) Engel, M. F. M.; Visser, A.; van Mierlo, C. P. M. *Langmuir* **2004**, *20*, 5530.
(12) Kuwajima, K. *FASEB J.* **1996**, *10*, 102.
(13) Kasemo, B. *Surf. Sci.* **2002**, *500*, 656.
(14) *Biopolymers at Interfaces*, 2nd ed.; Malmsten, M., Ed.; Marcel Dekker, Inc.: New York, 2003; Vol. 110.
(15) Tkachenko, A. G.; Xie, H.; Coleman, D.; Glomm, W.; Ryan, J.; Anderson, M. F.; Franzen, S.; Feldheim, D. L. *J. Am. Chem. Soc.* **2003**, *125*, 4700.
(16) Tkachenko, A. G.; Xie, H.; Liu, Y. L.; Coleman, D.; Ryan, J.; Glomm, W. R.; Shipton, M. K.; Franzen, S.; Feldheim, D. L. *Bioconjugate Chem.* **2004**, *15*, 482.
(17) Hemmersam, A. G.; Foss, M.; Chevallier, J.; Besenbacher, F. *Colloids Surf. B-Biointerfaces* **2005**, *43*, 208.
(18) Marx, K. A. *Biomacromolecules* **2003**, *4*, 1099.
(19) Sauerbrey, G. *Z. Phys.* **1959**, *155*, 206.
(20) Hook, F.; Kasemo, B.; Nylander, T.; Fant, C.; Sott, K.; Elwing, H. *Anal. Chem.* **2001**, *73*, 5796.
(21) Hook, F.; Voros, J.; Rodahl, M.; Kurrat, R.; Boni, P.; Ramsden, J. J.; Textor, M.; Spencer, N. D.; Tengvall, P.; Gold, J.; Kasemo, B. *Colloids Surf. B-Biointerfaces* **2002**, *24*, 155.
(22) Voros, J. *Biophys. J.* **2004**, *87*, 553.
(23) Turkevich, J.; Garton, G.; Stevenson, P. C. *J. Colloid Sci.* **1954**, *9*, S26.
(24) Turkevich, J.; Stevenson, P. C.; Hillier, J. *Discuss. Faraday Soc.* **1951**, 55.
(25) Turkevich, J.; Stevenson, P. C.; Hillier, J. *J. Phys. Chem.* **1953**, *57*, 670.
(26) Hidber, P. C.; Graule, T. J.; Gauckler, L. J. *J. Am. Ceram. Soc.* **1996**, *79*, 1857.
(27) Kelly, S. M.; Price, N. C. *Curr. Protein Pept. Sci.* **2000**, *1*, 349.
(28) Pace, C. N.; Vajdos, F.; Fee, L.; Grimsley, G.; Gray, T. *Protein Sci.* **1995**, *4*, 2411.
(29) Ahmad, F.; Bigelow, C. C. *J. Protein Chem.* **1986**, *5*, 355.
(30) Hook, F.; Rodahl, M.; Kasemo, B.; Brzezinski, P. *Proc. Natl. Acad. Sci. U.S.A.* **1998**, *95*, 12271.
(31) Su, X. D.; Zong, Y.; Richter, R.; Knoll, W. *J. Colloid Interface Sci.* **2005**, *287*, 35.
(32) Haynes, C. A.; Norde, W. *Colloids Surf. B-Biointerfaces* **1994**, *2*, 517.
(33) Agasoster, A. V.; Halskau, O.; Fuglebakk, E.; Froystein, N. A.; Muga, A.; Holmsen, H.; Martinez, A. *J. Biol. Chem.* **2003**, *278*, 21790.
(34) Pike, A. C. W.; Brew, K.; Acharya, K. R. *Structure* **1996**, *4*, 691.
(35) Sugai, S.; Ikeguchi, M. Conformational Comparison between Alpha-Lactalbumin and Lysozyme. In *Advances in Biophysics*; Japan Scientific Soc Press: Tokyo, 1994; Vol. 30, p 37.
(36) Permyakov, E. A.; Berliner, L. J. *FEBS Lett.* **2000**, *473*, 269.
(37) Griko, Y. V.; Privalov, P. L. *J. Mol. Biol.* **1994**, *235*, 1318.
(38) Hildebrandt, P.; Stockburger, M. *Biochemistry* **1989**, *28*, 6710.
(39) Bychkova, V. E.; Dujsekina, A. E.; Klenin, S. I.; Tiktopulo, E. I.; Uversky, V. N.; Ptitsyn, O. B. *Biochemistry* **1996**, *35*, 6058.
(40) Moosavi-Movahedi, A. A.; Chamani, J.; Goto, Y.; Hakimelahi, G. H. *J. Biochem. (Tokyo)* **2003**, *133*, 93.
(41) Muga, A.; Mantsch, H. H.; Surewicz, W. K. *Biochemistry* **1991**, *30*, 7219.
(42) Spooner, P. J. R.; Watts, A. *Biochemistry* **1990**, *30*, 3880.
(43) Spooner, P. J. R.; Watts, A. *Biochemistry* **1990**, *30*, 3871.
(44) Qi, P. X.; Brown, E. M.; Farrell, H. M. *Trends Food Sci. Technol.* **2001**, *12*, 339.
(45) Sawyer, L.; Holt, C. *J. Dairy Sci.* **1993**, *76*, 3062.
(46) Farrell, H. M., Jr.; Qi, P. X.; Brown, E. M.; Cooke, P. H.; Tunick, M. H.; Wickham, E. D.; Unruh, J. J. *J. Dairy Sci.* **2002**, *85*, 459.
(47) Lodish, H.; Berk, A.; Matsudaira, P.; Kaiser, C. A.; Krieger, M.; Scott, M. P.; Zipursky, S. L.; Darnell, J. *Molecular Cell Biology*, 5th ed.; W. H. Freeman and Co.: New York, 2003.
(48) Uversky, V. N.; Narizhneva, N. V.; Ivanova, T. V.; Tomashevski, A. Y. *Biochemistry* **1997**, *36*, 13638.
(49) Brust, M.; Walker, M.; Bethell, D.; Schiffrin, D. J.; Whyman, R. *J. Chem. Soc., Chem. Commun.* **1994**, 801.
(50) Haynes, C. A.; Tamura, K.; Korfer, H. R.; Blanch, H. W.; Prausnitz, J. M. *J. Phys. Chem.* **1992**, *96*, 905.
(51) Creighton, T. E. *Proteins: Structures and Molecular Principles*; W. H. Freeman: New York, 1984.
(52) Holmberg, K.; Jönsson, B.; Kronberg, K.; Lindman, B. *Surfactants and Polymers in Aqueous Solutions*, 2nd ed.; John Wiley & Sons, Ltd.: West Sussex, 2003.
(53) Eggers, D. K.; Valentine, J. S. *J. Mol. Biol.* **2001**, *314*, 911.
(54) Eggers, D. K.; Valentine, J. S. *Protein Sci.* **2001**, *10*, 250.

(55) Norde, W.; Lyklema, J. *J. Colloid Interface Sci.* **1978**, *66*, 295.
(56) Norde, W.; Lyklema, J. *J. Colloid Interface Sci.* **1979**, *71*, 350.
(57) Rodland, I.; Halskau, O.; Martinez, A.; Holmsen, H. *Biochim. Biophys. Acta-Biomembranes* **2005**, *1717*, 11.
(58) Kamerzell, T. J.; Unruh, J. R.; Johnson, C. K.; Middaugh, C. R. *Biochemistry* **2006**, *45*, 15288.
(59) Halskau, O.; Underhaug, J.; Froystein, N. A.; Martinez, A. *J. Mol. Biol.* **2005**, *349*, 1072.
(60) Halskau, O.; Froystein, N. A.; Muga, A.; Martinez, A. *J. Mol. Biol.* **2002**, *321*, 99.
(61) Dunker, A. K.; Lawson, J. D.; Brown, C. J.; Williams, R. M.; Romero, P.; Oh, J. S.; Oldfield, C. J.; Campen, A. M.; Ratliff, C. R.; Hipps, K. W.; Ausio, J.; Nissen, M. S.; Reeves, R.; Kang, C. H.; Kissinger, C. R.; Bailey, R. W.; Griswold, M. D.; Chiu, M.; Garner, E. C.; Obradovic, Z. *J. Mol. Graphics Modell.* **2001**, *19*, 26.
(62) Johnson, J. E.; Xie, M.; Singh, L. M.; Edge, R.; Cornell, R. B. *J. Biol. Chem.* **2003**, *278*, 514.
(63) Bychkova, V. E.; Pain, R. H.; Ptitsyn, O. B. *FEBS Lett.* **1988**, *238*, 231.
(64) Endo, T.; Martin Eilerss; Schatz, G. *J. Biol. Chem.* **1989**, *254*, 2951.
(65) Endo, T.; Schatz, G. *EMBO J.* **1988**, *7*, 1153.
(66) Jordi, W.; Li-Xin, Z.; Pilon, M.; Deme, R. A.; Kruijff, B. d. *J. Biol. Chem.* **1989**, *264*, 2292.
(67) Dunker, A. K.; Ensign, L. D.; Arnold, G. E.; Roberts, L. M. *FEBS Lett.* **1991**, *292*, 275−278.
(68) Griffith, J.; Manning, M.; Dunn, K. *Cell* **1981**, *23*, 747−753.
(69) Manning, M.; Chrysogelos, S.; Griffith, J. *Biophys. J.* **1982**, *37*, 28−30.
(70) Oh, J. S.; Davies, D. R.; Lawson, J. D.; Arnold, G. E.; Dunker, A. K. *J. Mol. Biol.* **1999**, *287*, 449.
(71) Watts, A. *Biochem. Soc. Trans.* **1995**, *23*, 959.
(72) Gasset, M.; Pozo, A. M. D.; Onaderra, M.; Gavilanes, J. G. *Biochem. J.* **1989**, *258*, 569.
(73) Johnson, J. E.; Cornell, R. B. *Mol. Membr. Biol.* **1999**, *16*, 217.
(74) Rytomaa, M.; Mustonen, P.; Kinnunen, P. K. J. *J. Biol. Chem.* **1992**, *267*, 22243.